Dynamics of a falling film with solutal Marangoni effect

Antonio Pereira and Serafim Kalliadasis
Department of Chemical Engineering, Imperial College London, London SW7 2AZ, United Kingdom
(Received 10 March 2008; revised manuscript received 24 June 2008; published 15 September 2008)

We investigate the dynamics of a thin liquid film on an inclined planar substrate in the presence of an insoluble surfactant on its free surface. We consider both the linear and nonlinear regimes. The linear regime is examined through the Orr-Sommerfeld eigenvalue problem of the full Navier-Stokes and concentration equations and wall and free-surface boundary conditions. The nonlinear regime is investigated through two different models. The first one is obtained from the classical long-wave expansion and the second one through an integral-boundary-layer approximation combined with a simple Galerkin projection. Although accurate close to the instability threshold, the first model fails to describe the dynamics of the system far from criticality. On the other hand, the second model not only captures accurately the behavior close to the instability threshold, but is also valid far from criticality. Analytical and numerical results on the role of the surfactant on the free-surface dynamics are presented. In the linear regime, the Marangoni stresses induced by the surfactant reduce the domain of instability for the base flow. In the nonlinear regime, the system evolves into solitary pulses for both the free surface and surfactant concentration. The amplitude and velocity of these pulses decrease as the Marangoni effect becomes stronger.

DOI: 10.1103/PhysRevE.78.036312 PACS number(s): 47.15.gm, 47.35.−i, 47.55.dk, 47.55.N−

I. INTRODUCTION

The dynamics of a thin film falling down an inclined planar substrate has been the subject of numerous studies since the pioneering works by Kapitza [1] and Kapitza and Kapitza [2]. A falling film is a convectively unstable open-flow hydrodynamic system with a sequence of wave instabilities and transitions which are generic to a large class of hydrodynamic and other nonlinear systems: amplification of small-amplitude white noise, filtering mechanism of linear instability, secondary modulation instability that converts the primary wave field into a train of solitary pulses, and inelastic pulse-pulse interaction. Extensive reviews of the rich dynamics of this system are given in [3,4].

The dynamics of a falling film can be influenced by surface tension gradients due to spatially inhomogeneous temperature fields (thermal Marangoni effect) or due to the presence of surface active agents—i.e., surfactants (solutal Marangoni effect). Both effects alter the fluid flow through interfacial stresses induced by changes of the surface tension of the fluid. The coupling of a falling film with the thermal Marangoni effect has been investigated in different settings. Goussis and Kelly [5] scrutinized the onset of the instability for a film falling down a uniformly heated wall, while Joo *et al.* [6], Kalliadasis *et al.* [7], Trevelyan and Kalliadasis [8], Ruyer-Quil *et al.* [9], and Scheid *et al.* [10] focused on the nonlinear wave regime for the same problem. Scheid *et al.* [11] investigated the nonlinear evolution of a falling film heated nonuniformly from below, while Demekhin *et al.* [12] examined the linear stability of a falling film heated by a downstream linearly increasing temperature distribution. On the other hand, Trevelyan *et al.* [13] and Trevelyan and Kalliadasis [14,15] studied the dynamics of a falling film in the presence of internal heat generation due to exothermic chemical reactions.

The associated problem of the coupling of a falling film with the solutal Marangoni effect has also been investigated in different settings. The influence of soluble surfactants on the linear instability of a falling film was examined by Ji and Setterwall [16] and Shkadov *et al.* [17]. On the other hand, the influence of insoluble surfactants on the linear instability of a falling film was examined by Blyth and Pozrikidis [18] while the coupling of a film falling down a corrugated wall with insoluble surfactants was examined by Pozrikidis [19] and Luo and Pozrikidis [20] in the limit of vanishing Reynolds number and by Luo and Pozrikidis [21] for finite Reynolds number.

In the present study we consider the problem of a film falling down a planar vertical wall in the presence of insoluble surfactants and in the region of small to moderate Reynolds numbers. We examine in detail the linear stability properties of the system by performing a systematic analysis of the Orr-Sommerfeld eigenvalue problem of the full Navier-Stokes and concentration equations. The same problem was also considered by Blyth and Pozrikidis [18] who identified all modes of the Orr-Sommerfeld problem: the usual interfacial mode for a free-falling film, a concentration mode, and the shear modes associated with the Nusselt semiparabolic velocity profile. They performed a small-wave-number expansion for the interfacial mode that also yields the critical Reynolds number for the instability onset, and they showed that the Marangoni effect can suppress the interfacial mode. They presented numerical results for the interfacial and concentration modes for small Reynolds numbers and for the leading shear mode at large Reynolds numbers. Here we give small-wave-number expansions for all modes, we present numerically all modes for both small and large Reynolds numbers, and we study the effect of the Marangoni number on all modes. We provide physical insight into the concentration mode and show that it is simply a "diffusional" mode appropriately modified by advection and is associated with the specific structure of the surface transport equation: this mode exists even in the absence of the Marangoni effect—i.e., for any species on the free sur-

face and not necessarily a surfactant or even if concentration is replaced with temperature.

We subsequently focus on the nonlinear dynamics following the destabilization of the base flow and clarify how it can be affected by the Marangoni stresses: the nonlinear regime has not been investigated before, and thus we provide a more integrated picture of the dynamics of a film with insoluble surfactant. Our starting point of the analysis of this regime is the "boundary-layer equations" in the presence of surfactant. These equations are derived with the "boundary-layer approximation" in which the pressure is eliminated by integrating across the film the cross-stream component of the momentum equation where the inertia effects are neglected. We then use the boundary-layer equations as a basis for the derivation of two reduced models: the first one is based on the classical long-wave expansion and the second one on a simple weighted residuals approach.

We first examine the linear stability characteristics of the two models. Both predict accurately the critical Reynolds number for the instability onset, and their neutral stability curves are found to be in good agreement with those obtained from the Orr-Sommerfeld problem (with the curves of the second model performing better than those of the first one). Subsequently we focus on single-hump stationary solitary waves. We demonstrate that for the first model the solitary wave solution branches for the speed of the waves as a function of Reynolds number are unrealistic with turning points and branch multiplicity at certain values of the Reynolds number above which solitary waves do not exist. This leads to a catastrophic blowup behavior for the first model when it is integrated in regions of the parameter space where solitary waves do not exist. In contrast, the solitary wave solution branches of the second prototype predict the continuing existence of solitary pulses for all Reynolds numbers. Moreover, the second prototype is found quite robust in time-dependent computations without any singularity formation. These computations also reveal that the large-time behavior of the system is characterized by trains of solitary-wave-like coherent structures which strongly resemble the infinite-domain stationary solitary waves.

Further, we scrutinize the role of the Marangoni stresses in the nonlinear regime. Their main effect is to dampen the free-surface solitary pulses. On the other hand, at sufficiently large Reynolds numbers the flow tends to accumulate the surfactant at the front stagnation point of a recirculation zone forming beneath the primary solitary hump, leading to large values of the surfactant concentration there. This can be alleviated or even suppressed all together by increasing the Marangoni number. Hence the Marangoni effect induced by the surfactant has a dramatic effect both on the linear and nonlinear regimes of the system.

The paper is organized as follows. In Sec. II we formulate the problem, and in Sec. III we give the nondimensionalization and governing dimensionless groups and their parametrization. The Orr-Sommerfeld eigenvalue problem for the linear stability of the base flow is examined in Sec. IV. In Sec. V we develop the boundary-layer equations in the presence of surfactant as a basis for the derivation of the two prototypes of reduced dimensionality discussed earlier. Numerical results for infinite-domain stationary solitary pulses are presented in Sec. VI, and time-dependent computations are discussed in Sec. VII.

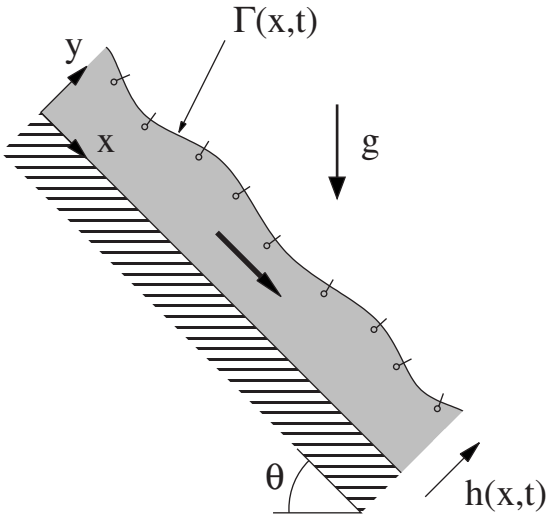

FIG. 1. Sketch of a film falling down a planar inclined substrate. The film thickness is $h(x,t)$ with respect to a Cartesian coordinate system (x,y) with origin on the substrate. The surface of the film is covered with an insoluble surfactant with concentration $\Gamma(x,t)$.

II. PROBLEM DEFINITION AND GOVERNING EQUATIONS

Figure 1 shows the problem definition. We consider a two-dimensional thin liquid film falling down a planar inclined wall forming an angle θ with the horizontal direction. The surface of the film is covered by insoluble surfactants which alter the surface tension, which in turn generates an interfacial shear stress that affects the evolution of the film.

A Cartesian coordinate system (x,y) is chosen so that x is in the direction parallel to the substrate and y is the outward-pointing coordinate normal to the substrate. The fluid has viscosity μ, density ρ, and surface tension σ. The governing equations are the continuity and Navier-Stokes equations

$$\boldsymbol{\nabla}\cdot\mathbf{u}=0, \tag{1a}$$

$$\rho\left(\frac{\partial}{\partial t}+\mathbf{u}\cdot\boldsymbol{\nabla}\right)\mathbf{u}=-\boldsymbol{\nabla}p+\boldsymbol{\nabla}\cdot\boldsymbol{\tau}+\rho\mathbf{g}, \tag{1b}$$

where $\boldsymbol{\nabla}=(\partial/\partial x,\partial/\partial y)$ is the gradient operator on the (x,y) plane, $\mathbf{u}=(u,v)$ is the fluid velocity vector, $\mathbf{g}=g(\sin\theta,-\cos\theta)$ with g is the gravitational acceleration, p is the fluid pressure, and $\boldsymbol{\tau}=\mu[(\boldsymbol{\nabla}\mathbf{u})+(\boldsymbol{\nabla}\mathbf{u})^t]$ is the deviatoric stress tensor.

These equations are subject to the following boundary conditions. On the substrate we have the usual no-slip and no-penetration conditions

$$\mathbf{u}=\mathbf{0} \quad \text{on} \quad y=0. \tag{2}$$

On the free surface $y=h(x,t)$ we have the kinematic boundary condition along with the normal and tangential stress balances

$$h_t + uh_x = v, \quad p_0 - p + (\boldsymbol{\tau}\cdot\mathbf{n})\cdot\mathbf{n} = 2\sigma K(h),$$
$$(\boldsymbol{\tau}\cdot\mathbf{n})\cdot\mathbf{t} = \nabla_s\sigma\cdot\mathbf{t}, \tag{3}$$

where p_0 is the pressure of the surrounding gas phase and $\mathbf{n}$ and $\mathbf{t}$ are unit vectors, normal (outward pointing) and tangential to the interface, respectively, defined from $\mathbf{n}=n^{-1}(-h_x,1)$ and $\mathbf{t}=n^{-1}(1,h_x)$, where $n=(1+h_x^2)^{1/2}$. $K(h)=-(1/2)\nabla_s\cdot\mathbf{n}$ is the mean curvature of the interface, and $\nabla_s=(\mathbf{I}-\mathbf{nn})\cdot\nabla$ is the surface gradient operator with $\mathbf{I}$ the 2×2 unitary matrix and $\mathbf{nn}$ the dyadic product of the unit vector $\mathbf{n}$ with itself. Hence the tangential stress balance includes the Marangoni effect in its right-hand side through the gradient of the surface tension along the interface.

So far, we have not specified the nature of the Marangoni effect and indeed Eqs. (1)–(3) apply to both thermal and solutal Marangoni effects. For the second case considered here the interfacial concentration Γ of the surfactant obeys the following transport equation at $y=h(x,t)$ [22,23]:

$$\Gamma_t + u\Gamma_x + \Gamma\nabla_s\cdot\mathbf{u} = D_s\nabla_s^2\Gamma, \tag{4}$$

where D_s is the surface diffusivity. The first two terms in this equation correspond to the material derivative of Γ as it is advected by the flow, the third term accounts for the concentration change due to the stretching of the surface, and the last term describes the surface diffusion of the surfactant, which is assumed to be given by Fick's law. The surfactant transport equation given in Ref. [24] can be rewritten as Eq. (4) in this paper provided that the partial time derivative in this reference is not interpreted as the usual partial time derivative—i.e., the derivative obtained by differentiating with respect to time for a fixed point in space—but as a partial time derivative that follows the interface in a direction normal to the interface (the "normal time derivative following the interface" according to the terminology by Cermelli *et al.* [25]). This issue is discussed in detail in Ref. [23].

The system is closed with a constitutive relation for the dependence of the surface tension on surfactant concentration, which then allows the evaluation of the right-hand side of the tangential stress balance in (3). Here we assume that for the region of concentrations of interest σ is a linear function of Γ,

$$\sigma = \sigma_0 - \gamma(\Gamma - \Gamma_0), \tag{5}$$

where Γ_0 is a uniform reference value corresponding to the Nusselt flat-film solution (given in Sec. III), $\sigma_0=\sigma(\Gamma_0)$, and $\gamma>0$ (for typical liquids). Equation (5) depends only on γ and Γ_0 and is a simple generic prototype equation of state that has been used frequently in thin-film studies to model the solutal Marangoni effect (see, e.g., the reviews in [26,27]). Indeed on several occasions the variation of surface tension with concentration found experimentally can be approximated by a linear function for a wide range of concentrations [28].

At the same time, various more involved models based on physicochemical and thermodynamic considerations have been suggested [29]. A widely used one is a nonlinear constitutive equation, the von Szyszkowski equation (e.g., [30–34]), which predicts a decrease of surface tension with surfactant concentration and reads

$$\sigma = \sigma_\mathrm{p} + RT\Gamma_\infty \ln\left(1 - \frac{\Gamma}{\Gamma_\infty}\right), \tag{6}$$

where σ_p is the surface tension of the pure liquid, R is the ideal gas constant, T is the absolute temperature, and Γ_∞ is the limiting surface concentration for the surfactant corresponding to a close-packed monolayer of molecules (saturation concentration). We now show that under certain conditions, Eq. (5) can be obtained from Eq. (6). We first note that Eq. (6) is not valid for large values of Γ, especially as Γ approaches Γ_∞ where σ develops a logarithmic singularity. Indeed, large values of Γ will induce strong changes of the mechanical properties of the interface and interfacial quantities such as surface viscosity must be taken into account. Γ is then assumed to be small to moderate, formally expressed as $\Gamma<\Gamma_\infty$ (a small value of Γ can still yield an appreciable Marangoni effect, but a very small value does not, and the situation would be equivalent to that of a free-falling film). Moreover, in order to simplify the constitutive model, Γ is assumed to be sufficiently close to the uniform reference value Γ_0 corresponding to the Nusselt flat-film solution (given in Sec. III). Hence Γ_0 is at most moderate as well. Let us then rewrite Eq. (6) as

$$\sigma = \sigma_\mathrm{p} + RT\Gamma_\infty \ln\left(1 - \frac{\Gamma_0}{\Gamma_\infty} - \frac{\Gamma-\Gamma_0}{\Gamma_\infty}\right)$$
$$= \sigma_\mathrm{p} + RT\Gamma_\infty\left[\ln\left(1 - \frac{\Gamma_0}{\Gamma_\infty}\right) + \ln\left(1 - \frac{\Gamma-\Gamma_0}{\Gamma_\infty-\Gamma_0}\right)\right],$$

which when expanded for $\Gamma-\Gamma_0 \ll \Gamma_\infty-\Gamma_0$ (which with Γ_0 at most moderate is equivalent to $\Gamma-\Gamma_0 \ll \Gamma_\infty$; i.e., the expansion takes place around Γ_0), yields the linear form in (5) where

$$\sigma_0 = \sigma_\mathrm{p} + RT\Gamma_\infty \ln\left(1 - \frac{\Gamma_0}{\Gamma_\infty}\right) \equiv \sigma(\Gamma_0) \tag{7a}$$

and

$$\gamma = \frac{RT\Gamma_\infty}{\Gamma_\infty - \Gamma_0}, \tag{7b}$$

thus allowing a connection with physical experiments. Note that γ depends on concentration through the ratio Γ_0/Γ_∞ with the value $RT/[1-(\Gamma_0/\Gamma_\infty)]$, while for very small Γ_0 compared to Γ_∞, γ has the value RT for all surfactants.

Falling film experiments typically involve a thin film of water at room temperature (25 °C) [35]. This was the case, for example, in the experimental studies by the Kapitzas on the dynamics of the free surface of the film [2]. Typical values of the various physical parameters for water are given in Table I. Various surfactants can then be used to examine the solutal Marangoni effect on the falling film, including soluble ones, provided that the time scale of desorption is small compared to the typical time scale of the dynamics considered here. This is, e.g., the case with sodium dodecyl sulfate on water, which is practically an insoluble surfactant [31,36]. Typical values of the various dimensional parameters for the surfactant are also given in Table I. The value for Γ_∞ is a basic reference value corresponding to a typical

TABLE I. Typical values of the various dimensional quantities. The working liquid is water at 25 °C, and the plane is vertical. For a fixed surfactant then the only free parameter is the Nusselt flat-film thickness, which can be modified via the flow rate $q_0=g\sin\theta h_0^3/(3\nu)$ (see discussion in Sec. III). Here it is assumed to be in the range ~0.1–1 mm, which is typical of free-falling film experiments [35].

Parameter	Symbol	Typical value
Nusselt flat-film thickness	h_0	0.1–1 mm
Nusselt flat-film interfacial velocity	u_0	0.05–5 m s^{-1}
Inclination angle	θ	90°
Liquid density [37]	ρ	$\approx 10^3$ kg m^{-3}
Liquid viscosity [37]	μ	$\approx 10^{-3}$ Pa s
Liquid surface tension [37]	σ_0	70–74 mN m^{-1}
Surfactant concentration	Γ_0	$0-2\times 10^{-7}$ mol m^{-2}
Surfactant maximum concentration [29,38]	Γ_∞	2×10^{-6} mol m^{-2}
Surface tension coefficient	γ	2400–2800 N m mol^{-1}
Surfactant surface diffusion coefficient [28]	D_s	10^{-10}–10^{-8} m^2 s^{-1}

order of magnitude; e.g., values $\Gamma_\infty=6\times 10^{-6}$ mol m^{-2} and 8×10^{-6} mol m^{-2} have also been reported [29] so that $\Gamma_\infty=\mathcal{O}(10^{-6}$ mol $m^{-2})$ (equivalently the value in Table I is a lower bound on Γ_∞). The range of values for Γ_0 is obtained by assuming Γ_0 to be a fraction of Γ_∞, $\Gamma_0=0-0.1\Gamma_\infty$, with $\sigma_0\sim 2800$ N m mol^{-1} for $\Gamma_0=0.1\Gamma_\infty$. The fraction 0.1 of Γ_∞ corresponds to a small value of Γ_0 which as pointed out earlier can still yield an appreciable Marangoni effect. Finally, the surface tension coefficient γ in Table I is obtained from Eq. (7b).

III. NONDIMENSIONALIZATION

The system (1)–(4) has a trivial solution corresponding to the plane-parallel base state, the Nusselt flat film with a semiparabolic velocity profile, a linear decreasing pressure distribution from the wall to the free surface, and a uniform surfactant concentration,

$$h=h_0,\quad u=\frac{g\sin\theta}{2\nu}(2h_0y-y^2),\quad v=0,$$
$$p=p_0+\rho g\cos\theta(h_0-y),\quad \Gamma=\Gamma_0, \tag{8}$$

with Γ_0 corresponding to the uniform surface tension σ_0 in Eq. (5). The volumetric flow rate (per unit width in the transverse direction) is obtained from $q_0=\int_0^{h_0}u\,dy=g\sin\theta h_0^3/(3\nu)$. We now utilize the trivial solution to introduce the nondimensionalization,

$$(x,y)\to h_0(x,y),\quad h\to h_0h,\quad (u,v)\to u_0(u,v),\quad t\to\frac{h_0}{u_0}t, \tag{9a}$$

$$p\to p_0+\rho g h_0\sin\theta p,\quad \Gamma\to\Gamma_0\Gamma, \tag{9b}$$

where $u_0=gh_0^2\sin\theta/(2\nu)$ is the Nusselt flat-film interfacial velocity.

In terms of these nondimensional variables Eqs. (1) become

$$u_x+v_y=0, \tag{10a}$$

$$\mathrm{Re}(u_t+uu_x+vu_y)=-2p_x+u_{xx}+u_{yy}+2, \tag{10b}$$

$$\mathrm{Re}(v_t+uv_x+vv_y)=-2p_y+v_{xx}+v_{yy}-2\cot\theta. \tag{10c}$$

These equations are subject to the wall boundary conditions

$$u=v=0\quad\text{on}\quad y=0 \tag{11}$$

and the dimensionless versions of the interfacial boundary conditions on $y=h(x,t)$ in (3):

$$v=h_t+uh_x, \tag{12a}$$

$$p+\frac{1}{1+h_x^2}[(1-h_x^2)u_x+h_x(u_y+v_x)]=-[\mathrm{We}-\mathrm{Ma}(\Gamma-1)]\frac{h_{xx}}{(1+h_x^2)^{3/2}}, \tag{12b}$$

$$-4h_xu_x+(1-h_x^2)(u_y+v_x)=-2\mathrm{Ma}\sqrt{1+h_x^2}\Gamma_x. \tag{12c}$$

On the interface we also have the dimensionless version of the surface transport equation (4):

$$\Gamma_t+u\Gamma_x+\frac{\Gamma}{1+h_x^2}[(u_x+h_xv_x)+h_x(u_y+h_xv_y)]=\frac{1}{\mathrm{Pe}_s}\frac{1}{\sqrt{1+h_x^2}}\left(\frac{\Gamma_x}{\sqrt{1+h_x^2}}\right)_x. \tag{13}$$

The basic equations for the analysis to follow are (10)–(13). This system is governed by θ and four dimensionless groups, the Reynolds, surface Péclet, Weber, and Marangoni numbers, respectively,

TABLE II. Typical ranges for the dimensionless groups corresponding to the parameter values given in Table I.

Dimensionless group	Symbol	Typical value
Modified Reynolds number	χ	10–10000
Kapitza number	Ka	3400
Schmidt number	Sc	100–10000
Modified Marangoni number	M	0–30
Reynolds number	Re	5–5000
Weber number	We	10–1000
Surface Péclet number	Pe_s	$500-5\times10^7$
Marangoni number	Ma	0–6

$$\mathrm{Re}=\frac{\chi}{2}\sin\theta,\quad \mathrm{Pe}_s=\frac{\chi}{2}\mathrm{Sc}\sin\theta,$$

$$\mathrm{We}=\frac{\mathrm{Ka}}{\chi^{2/3}\sin\theta},\quad \mathrm{Ma}=\frac{M}{\chi^{2/3}\sin\theta}, \tag{14a}$$

where

$$\chi=\frac{gh_0^3}{\nu^2},\quad \mathrm{Sc}=\frac{\nu}{D_s},\quad \mathrm{Ka}=\frac{\sigma_0}{\rho g^{1/3}\nu^{4/3}},\quad M=\frac{\gamma\Gamma_0}{\rho g^{1/3}\nu^{4/3}} \tag{14b}$$

correspond to a modified Reynolds number, Schmidt number, Kapitza number, and modified Marangoni number, respectively. With the exception of χ, all other parameters in Eq. (14b) are independent of h_0, which is a flow control parameter, and depend on the physical properties of the liquid-surfactant system (in experiments the film thickness can easily be modified via the flow rate q_0 and hence it is useful to have only one parameter that depends on the Nusselt flat-film thickness). Hence the above parametrization distinguishes clearly between the flow and the physical properties of the liquid and surfactant such that for a given liquid and surfactant the only free parameters are χ or h_0, and θ, while the vertical falling film-problem is a one-parameter system only.

Typical ranges of the dimensionless groups for the values of the dimensional parameters in Table I are given in Table II. Recall from Sec. II that a small ratio Γ_0/Γ_∞ can still cause a significant Marangoni effect. Indeed, from Table II the modified Marangoni number M can be as large as ~ 30 corresponding to $\gamma\sim 2800$ N m mol^{-1} and $\Gamma_0/\Gamma_\infty\sim 0.1$. Further, from the definitions of M and γ,

$$M=\frac{RT}{\rho g^{1/4}\nu^{4/3}}\frac{\Gamma_\infty}{\frac{\Gamma_\infty}{\Gamma_0}-1},$$

so that for the fixed value of Γ_∞ in Table I, M varies only as a function of the ratio Γ_0/Γ_∞ and for a fixed value of this ratio it does not depend on the surfactant, like γ (assuming the von Szyszkowski model is valid).

IV. LINEAR STABILITY OF THE NUSSELT FLAT FILM SOLUTION

A. Orr-Sommerfeld eigenvalue problem

We now examine the linear stability of the Nusselt flat-film solution in (8) whose dimensionless form is

$$u=2y-y^2,\quad v=0,\quad p=(1-y)\mathrm{cotan}\,\theta,\quad h=1,\quad \Gamma=1, \tag{15}$$

corresponding to the steady state of the system in (10)–(13). By substituting

$$u=2y-y^2+\tilde{u},\quad v=\tilde{v},\quad p=(1-y)\mathrm{cotan}\,\theta+\tilde{p},$$

$$h=1+\tilde{h},\quad \Gamma=1+\tilde{\Gamma} \tag{16}$$

into (10)–(13) and linearizing for $\tilde{h},\tilde{u},\tilde{v},\tilde{p},\tilde{\Gamma}\ll 1$ yields the disturbance equations

$$\tilde{u}_x+\tilde{v}_y=0, \tag{17a}$$

$$\mathrm{Re}[\tilde{u}_t+(2y-y^2)\tilde{u}_x+2(1-y)\tilde{v}]=-2\tilde{p}_x+\tilde{u}_{xx}+\tilde{u}_{yy}, \tag{17b}$$

$$\mathrm{Re}[\tilde{v}_t+(2y-y^2)\tilde{v}_x]=-2\tilde{p}_y+\tilde{v}_{xx}+\tilde{v}_{yy}, \tag{17c}$$

subject to the wall boundary conditions

$$\tilde{u}=\tilde{v}=0\quad \text{on}\quad y=0 \tag{18}$$

and the interfacial conditions along with the linearized concentration equation at $y=1$:

$$\tilde{v}=\tilde{h}_t+\tilde{h}_x, \tag{19a}$$

$$\tilde{p}+\tilde{u}_x=-\mathrm{We}\tilde{h}_{xx}+\tilde{h}\,\mathrm{cotan}\,\theta, \tag{19b}$$

$$-2\tilde{h}+\tilde{u}_y+\tilde{v}_x=-2\mathrm{Ma}\tilde{\Gamma}_x, \tag{19c}$$

$$\mathrm{Pe}_s(\tilde{\Gamma}_t+\tilde{\Gamma}_x+\tilde{u}_x)=\tilde{\Gamma}_{xx}. \tag{19d}$$

The disturbances are sought in the form of normal modes

$$[\tilde{u},\tilde{v},\tilde{p},\tilde{h},\tilde{\Gamma}]=[U(y),V(y),P(y),H,G]\exp(\lambda t+ikx), \tag{20}$$

which introduce the functions $U(y)$, $V(y)$, and $P(y)$ and the constants H and G. k is the wave number, and the complex frequency $i\lambda=i\lambda_R-\lambda_I$ contains the growth rate λ_R and the complex wave velocity $c=i\lambda/k$, with $c_R=-\lambda_I/k$ the phase velocity. The disturbance equations are simplified by introducing the stream function $\Psi=\psi(y)\exp(\lambda t+ikx)$, with $\tilde{u}=\Psi_y$ or $U=\psi_y$ and $\tilde{v}=-\Psi_x$ or $V=-ik\psi$. Equations (17)–(19) are then converted into the Orr-Sommerfeld (OS) eigenvalue problem of the linearized Navier-Stokes and concentration equations

$$(D^2-k^2)^2\psi=\mathrm{Re}\{[\lambda+ik(2y-y^2)](D^2-k^2)+2ik\}\psi, \tag{21a}$$

subject to the boundary conditions at $y=0$,

$$\psi = 0, \quad D\psi = 0, \tag{21b}$$

and at $y=1$,

$$(\lambda + ik)(D^2 + k^2)\psi = -2ik\psi - 2k^2 \mathrm{Ma} D\psi + 2i\frac{\mathrm{Ma}}{\mathrm{Pe}_s}k^3 G, \tag{21c}$$

$$(D^2 - 3k^2)D\psi = (\lambda + ik)\mathrm{Re}\, D\psi + ik(\mathrm{cotan}\ \theta + k^2 \mathrm{We})[(D^2 + k^2)\psi + 2ik\mathrm{Ma}G], \tag{21d}$$

$$\left(\lambda + ik + \frac{k^2}{\mathrm{Pe}_s}\right)G = -ikD\psi, \tag{21e}$$

where $D \equiv d/dy$. Hence the OS eigenvalue problem contains two unknowns: $\psi(y)$, which satisfies the fourth-order differential equation (21a), and G, and is subject to five boundary conditions in Eqs. (21b)–(21e). The original variables P and H in Eq. (20) are obtained from

$$P = \frac{(D^2 - k^2)D\psi}{2ik} - \frac{\mathrm{Re}[\lambda + ik(2y - y^2)]D\psi}{2ik} + \mathrm{Re}(1-y)\psi, \tag{22a}$$

$$H = \frac{1}{2}(D^2 + k^2)\psi(1) + ik\mathrm{Ma}G. \tag{22b}$$

B. Small-wave-number expansion and critical condition

Although a full solution of (21) can only be obtained numerically, an analytical solution is possible in the limit $k \to 0$. As in (21) only odd powers have an imaginary coefficient, it is appropriate to seek a solution in the form

$$[\psi, G, \lambda] = [\psi_0, G_0, \lambda_0] + ik[\psi_1, G_1, \lambda_1] + k^2[\psi_2, G_2, \lambda_2] + [\mathcal{O}(k^3), \mathcal{O}(k^3), \mathcal{O}(k^3)],$$

where even terms in this expansion are real and odd purely imaginary. Substituting it into Eq. (21) and expanding in powers of k gives a sequential solution of the eigenvalue problem. The eigenvalue λ is obtained from the tangential stress balance, Eq. (21c), where the Marangoni effect is predominant. Note that the linearity and homogeneity of Eq. (21) leads to an infinite number of solutions; however, by appropriately normalizing ψ_0 and removing replicated solutions of ψ_0 that occur at each of the higher orders, we can obtain a unique solution. The result for λ is

$$\lambda^1(k) = -2ik + \left(\frac{8}{15}\mathrm{Re} - \frac{2}{3}\,\mathrm{cotan}\ \theta - 2\mathrm{Ma}\right)k^2 + \mathcal{O}(k^3), \tag{23a}$$

$$\lambda^2(k) = -ik - \frac{1}{\mathrm{Pe}_s}k^2 + \mathcal{O}(k^3), \tag{23b}$$

$$\lambda_n^3(k) = -\frac{\pi^2}{4\,\mathrm{Re}}n^2 + \mathcal{O}(k), \ n \text{ odd}, \tag{23c}$$

i.e., a countable infinite family of eigenvalues and where the superscripts 1, 2, and 3 are used to denote the three distinct types of modes. Note that the higher-order terms of $\mathcal{O}(k^3)$, $\mathcal{O}(k^3)$, and $\mathcal{O}(k)$ in (23a)–(23c), respectively, are not given here as the solution of the OS problem at the corresponding orders is rather cumbersome and lengthy [the equations do suggest though that Ma appears in $\mathcal{O}(k^3)$ in (23b) and $\mathcal{O}(k^2)$ in (23c)].

The second mode originates from the surface transport equation and was first obtained numerically by Blyth and Pozrikidis [18] in their study of the OS problem. They referred to it as the "Marangoni mode." Here we prefer the term "concentration mode" as the mode exists even for $\mathrm{Ma}=0$—i.e., for any species on the free surface and not necessarily a surfactant. In other words, this mode is not a feature of the coupling between the film flow and the surfactant. It is simply a "diffusional mode" appropriately modified by advection and is associated with the particular structure of the surface transport equation, which is just the Laplacian of Γ together with the convective terms and a term due to the stretching of the interface. This mode would be present independently of the particular situation being examined—e.g., for an horizontal film or even in the absence of a film—in which case the stretching term would disappear as there is no interface; of course, Γ would represent a different physical entity in each case.

Hence for the surfactant problem considered here the concentration mode is associated with the diffusion of the species and its advection by the flow as also indicated by the presence of Pe_s. The phase velocity for this mode is $c_R = -\lambda_I/k = 1 + \mathcal{O}(k^3)$; i.e., to leading order in k it is the same with the free-surface velocity of the Nusselt flat film (recall from Sec. III that velocities scale with the Nusselt flat-film interfacial velocity) so that the species is simply transported by the flow. This mode is strictly stable as long as the surfactant is able to diffuse; i.e., Pe_s is finite, but it becomes neutrally stable when $\mathrm{Pe}_s \to \infty$, in which case convection is much faster than diffusion and any perturbation in surfactant concentration does not decay, but is advected by the flow without any change.

The modes in (23c) are due to the hydrodynamics for $\mathrm{Ma}=0$. In this limit, these modes are the so-called "shear modes" associated with the semiparabolic Nusselt velocity profile [3,39] and we shall also refer to them as "shear modes" in the presence of the Marangoni effect. In the absence of the Marangoni effect these modes are stable in the limit $k \to 0$, but the least stable shear mode can be destabilized at some finite k. We shall demonstrate later on that the same is true in the presence of the Marangoni effect in agreement with the prediction by Blyth and Pozrikidis [18].

The first mode is also due to the hydrodynamics when $\mathrm{Ma}=0$. It is the classical long-wave interfacial instability mode first observed in the experiments by Kapitza and Kapitza [2] appropriately modified by the Marangoni effect and subsequently we shall refer to it as the "Kapitza mode." The threshold of this mode and its linear stability properties

were scrutinized by Benjamin [40] and Yih [41] in the absence of the Marangoni effect, by Benjamin [42], Whitaker [43], and Blyth and Pozrikidis [18] in the presence of the solutal Marangoni effect associated with insoluble surfactants, and by Goussis and Kelly [5], Kalliadasis *et al.* [7], Trevelyan and Kalliadasis [8], and Scheid *et al.* [10] in the presence of the thermocapillary Marangoni effect induced by heating the film uniformly from below. The real part of λ^1 indicates that the onset of instability occurs when the coefficient of $\mathcal{O}(k^2)$ vanishes, which gives the critical Reynolds number above which the flow loses stability,

$$\mathrm{Re}_c = \frac{5}{4}\,\mathrm{cotan}\,\theta + \frac{15}{4}\mathrm{Ma}, \tag{24}$$

while the maximum growing linear mode at criticality has a wave number that is exactly zero. Equation (24) coincides with the analytical prediction by Blyth and Pozrikidis [18] (following an appropriate transformation associated with the scalings adopted by these authors) and for Ma=0 reduces to the well-known critical condition for a free falling film, $\mathrm{Re}_c=(5/4)\mathrm{cotan}\,\theta$ [40,41]. The phase velocity of this mode is $c_R=2+\mathcal{O}(k^3)$; i.e., to leading order in k infinitesimal interfacial disturbances travel with a velocity twice that of the flat film interfacial velocity (again, recall from Sec. III that velocities scale with the Nusselt flat-film interfacial velocity).

The critical condition in (24) indicates that increasing Ma decreases Re_c and hence the Marangoni effect is stabilizing. The opposite would be true for $\mathrm{Ma}<0$—i.e., $\gamma<0$. Indeed, although typically surface tension decreases when concentration increases, there are some systems known to display the opposite behavior [31]. For simplicity we shall focus here on the usual case $\gamma>0$.

Finally, for the associated problem of thermocapillary Marangoni effect (with $\gamma>0$) on a falling film due to heating uniformly the film from below, the influence of the Marangoni effect is opposite to that in the present problem: it reduces the critical Reynolds number (by an amount proportional to both the thermocapillary Marangoni number and the Biot number that expresses the rate of heat transport at the liquid-gas interface) and hence it has a destabilizing influence on the film [5,7,8,10].

C. Numerical solution

The OS eigenvalue problem in (21) can be solved numerically by a variety of methods such as shooting, finite-differences, or spectral methods [18]. Here we utilize the continuation software AUTO97 by Doedel *et al.* [44] and based on Keller's pseudoarclength continuation method [45]. It is a powerful, fast, and efficient numerical software for solving equations whose solutions are subject to a set of constraints, and we have successfully implemented it before in the numerical solution of boundary value problems such as the OS problem that governs the linear stability of a falling film heated uniformly from below [10].

The numerical methodology of AUTO97 consists of constructing successive solutions of the equations by following continuously a branch in the parameter space. A set of constraints (including the boundary conditions) and the free parameters to vary have to be specified (the exact number depends on the dimensionality of the branch to be followed). A starting point for the continuation procedure is typically a trivial solution for the chosen values of the free parameters and which also satisfies all constraints.

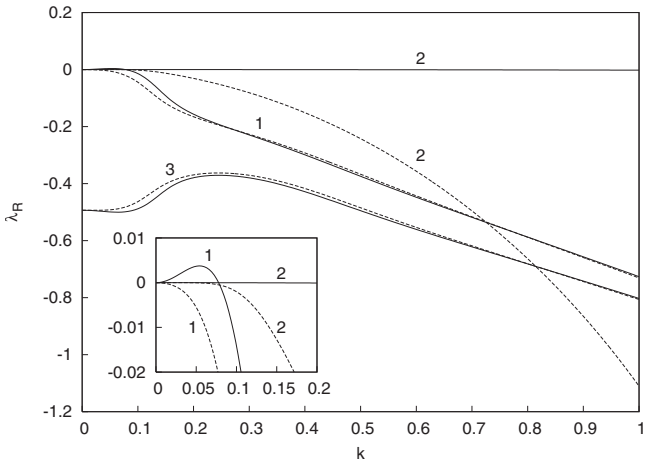

FIG. 2. Numerical solution of the Orr-Sommerfeld eigenvalue problem (21): dispersion curves $\lambda_R(k)$ of the three least stable modes as $k\to 0$ and two different values of the modified Marangoni number: $M=0$ (solid line) and $M=9$ (dashed line). The values of the remaining parameters are $\chi=10$, Ka=3000, Sc=100, and $\theta=\pi/2$. The curves marked with 1, 2, and 3 correspond to the Kapitza, concentration, and shear modes in (23). The inset is a blowup of the behavior as $k\to 0$. Note that the solid curve 2 for $M=0$ moves very slowly downwards as k increases, while curve 3 starts from $-\pi^2/(4\,\mathrm{Re})$ at $k=0$ [see (23c)].

As the system in (21) is linear, the amplitude of its solution is undetermined and so a constraint and normalization condition on the amplitude must be added. Here we choose the integral constraint

$$\int_0^1 (\psi+G)dy \equiv \int_0^1 \psi\,dy + G = 1, \tag{25}$$

as G is only defined on the interface and does not depend on y. The OS eigenvalue problem is then recast into a dynamical system of dimension 11: four complex ordinary differential equations or equivalently eight real ones for ψ plus $Dy=1$ to convert the nonautonomous dynamical system to an autonomous one plus two from $DG=0$ (recall that G is only defined on the interface and so its not influenced by y—we need to incorporate G in the dynamical system). This 11th-order dynamical system is subject to the integral constraint in (25). For a specific mode and set of parameter values, we use as a starting solution the one derived analytically in the limit $k\to 0$ as detailed earlier and k is chosen as the continuation parameter. The complex constraint in (25), equivalent to two real constraints, implies that two parameters are allowed to vary along the branches of solutions. These are chosen as the speed c and modified Reynolds number χ, and since k is the continuation parameter, the result of the computation is $c_R(k)$ and $\chi(k)$.

Figure 2 depicts the dispersion curves $\lambda_R(k)$ for the three least stable modes as $k\to 0$ (modes with largest λ_R in this

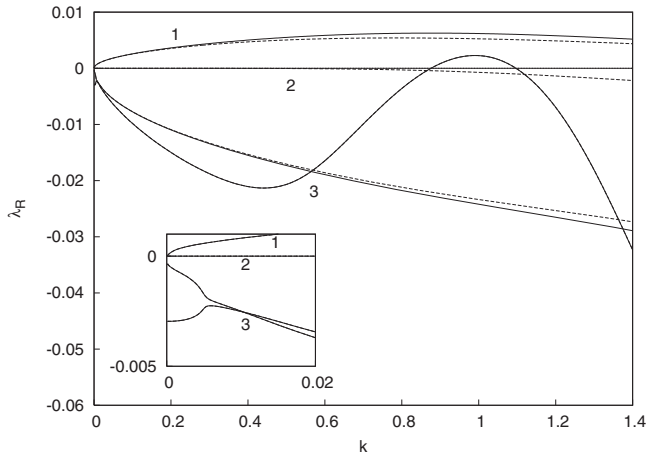

FIG. 3. Numerical solution of the Orr-Sommerfeld eigenvalue problem (21) for $\chi=1.5\times10^4$: dispersion curves $\lambda_R(k)$ of the four least stable modes as $k\to0$ and two different values of the modified Marangoni number: $M=0$ (solid line) and $M=9$ (dashed line). The values of the remaining parameters are the same with those in Fig. 2. The curves marked with 1, 2, and 3 correspond to the Kapitza, concentration, and shear modes for $n=1,3$ in (23). The inset is a blowup of the behavior as $k\to0$. In this region the $M=0$ and $M=9$ curves are graphically indistinguishable from each other. The shear modes for $n=1,3$ start from $-\pi^2/(4\mathrm{Re})$ and $-9\pi^2/(4\mathrm{Re})$ at $k=0$, respectively. These two modes cross over first at $k\simeq0.01$ and later on at $k\simeq0.6$. Note that for the $n=1$ shear mode the $M=0$ and $M=9$ curves are graphically indistinguishable from each other over the entire range of wave numbers. Note also that solid curve 2 for $M=0$ moves very slowly downwards as k increases.

region), $\chi=10$, and two values of the modified Marangoni number, $M=0$ and $M=9$. The values of the remaining parameters are Ka=3000 (water at 25°), Sc=100, and $\theta=\pi/2$ (these parameter values are fixed for the remaining of our study). The figure indicates that for $M=9$ the Marangoni effect makes the growth rate of the Kapitza mode negative for all k and hence it completely stabilizes this mode consistent with (23a); note, however, that in the region $k\simeq0.5$, the Marangoni effect amplifies the Kapitza mode and this is followed by a slow dampening at $k\simeq0.8$. Regarding the concentration mode, the Marangoni effect dampens it for all k. On the other hand, the shear modes in the presence of the Marangoni effect seem to be less stable up to $k\simeq0.8$ and are slowly dampened for larger k.

Figure 3 depicts the dispersion curves $\lambda_R(k)$ for the four least stable modes as $k\to0$, Kapitza mode, and concentration mode and the first two shear modes for $n=1$ and $n=3$, for the large value $\chi=1.5\times10^4$ and two values of the modified Marangoni number, $M=0$ and $M=9$. The first shear mode for $n=1$ dominates over the second one for $n=3$ as $k\to0$ and up to $k\simeq0.01$, but the second one dominates over the first one from $k\simeq0.01$ up to $k\simeq0.6$. The first shear mode then takes over the second one and is eventually destabilized at $k\simeq1$. This mode remains practically unaltered when M changes from 0 to 9. The growth rate of the Kapitza mode is the one that still dominates the instability. Equation (23c) shows that in the region of $k\to0$ and as Re tends to infinity, there will be an infinite number of shear modes clustered at the origin with vanishing growth rates there and potentially more shear modes might be destabilized as Re increases to values beyond that in Fig. 3. Finally we note that for the large value of χ in the figure, $\lambda_R^1\sim\mathrm{Re}k^2$ and one has to go to a really small k for the quadratic behavior of the Kapitza mode with respect to k to be visible.

V. MODEL EQUATIONS IN THE PRESENCE OF SURFACTANT

A. Boundary-layer equations

For a free-falling film the linear instability due to the Kapitza interfacial mode eventually leads, through a sequence of wave transitions, to a nonlinear regime which is typically characterized by trains of solitary pulses which continuously interact with each other. We shall demonstrate that the same is true for a falling film in the presence of surfactant.

The starting point of our analysis of the nonlinear wave regime is the "boundary-layer equations" in the presence of surfactant. The boundary-layer equations for a free-falling film are typically derived by assuming strong surface tension effects and without strict orders of magnitude assignments for the different dimensionless groups (see, e.g., [4,46]). These equations are obtained with the so-called "boundary-layer approximation": the pressure is typically eliminated, as in Prandtl's boundary-layer theory [47], by integrating the y component of the momentum equation in which the inertial effects are neglected across the film. The resulting pressure distribution is then substituted into the x component of the momentum equation.

The boundary-layer approximation is performed by assuming that the strong surface tension effects induce large wavelengths (in comparison with the Nusselt flat-film thickness h_0) and consequently a scale separation between x and y. Formally, we define a small parameter $\epsilon\sim\partial/\partial x,\partial/\partial t$, the "long-wave" or "film parameter," which allows us to investigate slow time and space modulations of the Nusselt flat-film solution. We then introduce the transformation

$$x\to\frac{x}{\epsilon},\quad t\to\frac{t}{\epsilon},\quad v\to\epsilon v, \tag{26}$$

which converts Eqs. (10) to

$$u_x+v_y=0, \tag{27a}$$

$$\epsilon\,\mathrm{Re}(u_t+uu_x+vu_y)=-2\epsilon p_x+\epsilon^2u_{xx}+u_{yy}+2, \tag{27b}$$

$$\epsilon^2\,\mathrm{Re}(v_t+uv_x+vv_y)=-2p_y+\epsilon^3v_{xx}+\epsilon v_{yy}-2\mathrm{cotan}\,\theta, \tag{27c}$$

subject to the wall boundary conditions

$$u=v=0\quad\text{on}\quad y=0 \tag{28}$$

and the rescaled versions of the interfacial boundary conditions (12):

$$v=h_t+uh_x, \tag{29a}$$

$$p + \frac{\epsilon}{1+\epsilon^2 h_x^2}[(1-\epsilon^2 h_x^2)u_x + h_x(u_y + \epsilon^2 v_x)] = -[\text{We-Ma}(\Gamma - 1)]\frac{\epsilon^2 h_{xx}}{(1+\epsilon^2 h_x^2)^{3/2}}, \tag{29b}$$

$$-4\epsilon^2 h_x u_x + (1-\epsilon^2 h_x^2)(u_y + \epsilon^2 v_x) = -2\epsilon \text{Ma}\sqrt{1+\epsilon^2 h_x^2}\,\Gamma_x. \tag{29c}$$

On the interface we also have the rescaled version of the surface transport equation (13):

$$\Gamma_t + u\Gamma_x + \frac{\Gamma}{1+\epsilon^2 h_x^2}[u_x + \epsilon^2 h_x v_x + h_x(u_y + \epsilon^2 h_x v_y)] = \frac{\epsilon}{\text{Pe}_s}\frac{1}{\sqrt{1+\epsilon^2 h_x^2}}\left(\frac{\Gamma_x}{\sqrt{1+\epsilon^2 h_x^2}}\right)_x. \tag{30}$$

With $\epsilon^2\text{Re} \ll 1$, the y component of the momentum equation (27c) is $p_y = -\text{cotan}\,\theta + \mathcal{O}(\epsilon, \epsilon^2\text{Re})$. Also, with $\text{Ma} \ll \text{We}$, $\epsilon^2\text{We}$ at most of $\mathcal{O}(1)$ and $\epsilon^2\text{We} \gg \epsilon$, the normal stress balance in (29b) gives $p = -\epsilon^2\text{We}h_{xx} + \mathcal{O}(\epsilon, \epsilon^2\text{Ma})$ on $y = h(x,t)$. With $\text{Re} \ll \text{We}$ the pressure is then given by $p = \text{cotan}\,\theta(h - y) - \epsilon^2\text{We}h_{xx} + \mathcal{O}(\epsilon, \epsilon^2\text{Re}, \epsilon^2\text{Ma})$, which is then substituted into the x component of the momentum equation (27b) and we neglect terms of $\mathcal{O}(\epsilon^2, \epsilon^3\text{Re}, \epsilon^3\text{Ma})$, but we keep the inertia terms which are of $\mathcal{O}(\epsilon\text{Re})$. Hence, ϵRe is at most of $\mathcal{O}(1)$ and $\epsilon\text{Re} \gg \{\epsilon^2, \epsilon^3\text{Ma}\}$, while $\epsilon^2\text{Re} \ll 1$ is automatically ensured by ϵRe at most of $\mathcal{O}(1)$. Further, in the tangential stress balance equation (29c) we assume ϵMa at most of $\mathcal{O}(1)$, $\epsilon\text{Ma} \gg \epsilon^2$ and we neglect terms of $\mathcal{O}(\epsilon^2, \epsilon^3\text{Ma}) = \mathcal{O}(\epsilon^2)$ since $\epsilon^3\text{Ma}$ is at most of $\mathcal{O}(\epsilon^2)$. At the same time since ϵRe is at most of $\mathcal{O}(1)$, the neglected terms in (27b) are of $\mathcal{O}(\epsilon^2, \epsilon^3\text{Re}, \epsilon^3\text{Ma}) = \mathcal{O}(\epsilon^2)$. Note that with ϵRe at most of $\mathcal{O}(1)$, ϵMa at most of $\mathcal{O}(1)$, and $\epsilon\text{We} \gg 1$, the conditions $\text{Re} \ll \text{We}$ and $\text{Ma} \ll \text{We}$ are automatically satisfied.

In the concentration equation (30) we assume $\epsilon/\text{Pe}_s \gg \epsilon^2$, ϵ/Pe_s at most of $\mathcal{O}(1)$ or equivalently $\text{Pe}_s \ll \epsilon^{-1}$, Pe_s at least of $\mathcal{O}(\epsilon)$, and we neglect terms of $\mathcal{O}(\epsilon^2)$. We note that for small Pe_s, the surfactant will have a uniform concentration: its motion is dominated by diffusion which is so fast compared to convection so that any peaks in surfactant concentration will be instantly homogenized [indeed in this limit and after neglecting terms of $\mathcal{O}(\epsilon^2)$, $\Gamma_{xx} = 0$ with solution $\Gamma = \text{const} \equiv 1$ as Γ has to be finite as $x \to \pm\infty$]. On the other hand, for large Pe_s the motion of the surfactant is dominated by convection as pointed out in Sec. IV B. The extent to which the surfactant affects the flow now through the Marangoni effect depends on the size of $\text{Ma}\Gamma_x$.

These assumptions then lead to the bulk equations

$$u_x + v_y = 0, \tag{31a}$$

$$\epsilon\,\text{Re}(u_t + uu_x + vu_y) = -2\epsilon h_x \text{cotan}\,\theta + 2\epsilon^3\text{We}h_{xxx} + u_{yy} + 2, \tag{31b}$$

subject to the wall boundary conditions

$$u = v = 0 \quad \text{on} \quad y = 0 \tag{32}$$

and interfacial boundary conditions

$$h_t + uh_x - v = 0, \tag{33a}$$

$$u_y = -2\epsilon\text{Ma}\Gamma_x, \tag{33b}$$

while the concentration equation is simplified to

$$\text{Pe}_s(\Gamma_t + u\Gamma_x + \Gamma u_x + \Gamma h_x u_y) = \epsilon\Gamma_{xx}. \tag{34}$$

Note that Eqs. (33a) and (34) can be written in conservative form as $h_t + q_x = 0$ and $\Gamma_t + [u|_{y=h}\Gamma - \epsilon\Gamma_x/\text{Pe}_s]_x = 0$, respectively, where $q = \int_0^h u\,dy$ is the flow rate in the streamwise direction.

Equations (31)–(34) are the first-order boundary-layer equations in the presence of surfactant [as terms of $\mathcal{O}(\epsilon^2)$ and higher have been neglected] and, much like the boundary-layer equations for a free-falling film, they are also derived with only the long-wave assumption and without precise and overly restrictive stipulations on the order of magnitude of the different dimensionless groups. They are the basis for the derivation of two simpler sets of equations in the following two subsections: namely, the equation obtained from the long-wave expansion and the integral-boundary-layer approximation.

B. Long-wave expansion

The free-boundary problem in (31)–(34) can be substantially simplified with a "long-wave" expansion (LWE)—i.e., a perturbation expansion in ϵ. For the free-falling film LWE leads to a single equation of the evolution type for the free surface (see, e.g., [3,4]). A detailed comprehensive review of LWE in different thin-film flow settings is given in [26], while applications of LWE on wetting-dewetting problems and isothermal and heated falling films specifically are given in [27].

We begin by assigning the following relative orders between the different dimensionless parameters and ϵ: $\text{Re} = \mathcal{O}(1)$, $\text{We} = \mathcal{O}(\epsilon^{-2})$, and $\text{Ma} = \mathcal{O}(1)$, consistent with the orders of magnitude assignments in Sec. V A. For Pe_s we retain the order of magnitude assignment in Sec. V A, i.e., $\epsilon/\text{Pe}_s \gg \epsilon^2$ and ϵ/Pe_s at most of $\mathcal{O}(1)$. We then expand u and v up to $\mathcal{O}(\epsilon)$, $\{u,v\} \sim \{u_0,v_0\} + \epsilon\{u_1,v_1\}$ [after all, in our boundary-layer equations we have neglected terms of $\mathcal{O}(\epsilon^2)$ and higher] and we substitute these expansions into (31), (32), and (33b) (note that Γ is not expanded with respect to ϵ and hence a precise order of magnitude for Pe_s is not required). The resulting set of equations is solved for u_0, u_1, v_0 and v_1 (the velocity and y dependence are thus eliminated from the boundary-layer equations) and by substituting the expansions for u and v into the kinematic boundary condition (33a) and the expansion for u into the concentration equation (34), we obtain a set of two, first-order in the long-wave parameter ϵ, coupled nonlinear partial differential equations for the evolution in time and space of h and Γ. The parameter ϵ can be scaled away from these equations by reverting to the original time and space variables—i.e., $x \to \epsilon x$ and $t \to \epsilon t$—which yields the final LWE model equations

$$h_t + \left(\frac{2}{3}h^3 - \frac{2}{3}\mathrm{cotan}\,\theta h^3 h_x + \frac{2}{3}\mathrm{We} h^3 h_{xxx} + \frac{8}{15}\,\mathrm{Re}\, h^6 h_x - \mathrm{Ma} h^2 \Gamma_x \right)_x = 0, \tag{35a}$$

$$\Gamma_t + \left[\left(h^2 - \mathrm{cotan}\,\theta h^2 h_x + \mathrm{We} h^2 h_{xxx} + \frac{5}{6}\,\mathrm{Re}\, h^5 h_x - 2\mathrm{Ma} h \Gamma_x \right)\Gamma - \frac{\Gamma_x}{\mathrm{Pe_s}} \right]_x = 0. \tag{35b}$$

A linear stability analysis of the steady state $[h,\Gamma]=[1,1]$ with perturbations of the form $\exp(\lambda t+ikx)$ yields two roots for λ, which when expanded for small k become

$$\lambda^1(k) = -2ik + \left(\frac{8}{15}\,\mathrm{Re} - \frac{2}{3}\mathrm{cotan}\,\theta - 2\mathrm{Ma} \right)k^2 + \left(\frac{7}{30}\,\mathrm{Re} - \frac{1}{3}\mathrm{cotan}\,\theta + \frac{2}{\mathrm{Pe_s}} \right)\mathrm{Ma} ik^3 + \mathcal{O}(k^4), \tag{36a}$$

$$\lambda^2(k) = -ik - \frac{1}{\mathrm{Pe_s}}k^2 - \left(\frac{7}{30}\,\mathrm{Re} - \frac{1}{3}\mathrm{cotan}\,\theta + \frac{2}{\mathrm{Pe_s}} \right)\mathrm{Ma} ik^3 + \mathcal{O}(k^4). \tag{36b}$$

By neglecting terms of $\mathcal{O}(k^3)$ and higher, these modes are identical to the Kapitza and concentration modes in (23a) and (23b) obtained from the OS eigenvalue problem [by neglecting terms of $\mathcal{O}(k^3)$ and higher]. As a consequence, LWE gives exactly the same critical condition with (24) obtained from the OS analysis. However, LWE fails to predict the shear modes in (23c): it is the y dependence in the OS eigenvalue problem that is responsible for the infinite number of modes. LWE eliminates this dependence by slaving all variables, except Γ, to h, yielding finally two evolution equations for h and Γ and hence only two linear modes.

C. Weighted-integral-boundary-layer approximation

Another way of eliminating the y dependence of the problem is via the "integral-boundary-layer" (IBL) approximation. For the free-falling film IBL was introduced by Shkadov [48] (Demekhin and Shkadov extended it to three dimensions [46], but here we are concerned with two-dimensional flows). It combines the first-order boundary-layer approximation with the assumption of a self-similar semiparabolic profile and the Kármán-Pohlhausen averaging method in boundary-layer theory in aerodynamics [47]. The first-order IBL approximation leads to a system of two coupled nonlinear partial differential equations for the film thickness and flow rate in the streamwise direction. This model has been successful in describing solitary waves in the region of moderate Reynolds numbers (e.g., [4]), but its prediction of the critical Reynolds number for the instability onset and of the neutral stability curve close to criticality have a 20% error compared to those obtained from OS.

In contrast, the LWE neutral curve agrees with the OS one for Re close to Re_c, but deviates from the OS one as Re increases. By including higher-order terms in LWE, this deviation is progressively delayed to higher Re. As LWE is a regular perturbation expansion of the full Navier-Stokes and other equations such as energy equation in the case of heated films, it also predicts accurately interfacial quantities such as interfacial temperature (LWE reduces all dependent variables to interfacial ones) close to criticality. Hence, LWE fully resolves the behavior close to the instability threshold. However, unlike the LWE neutral curve which can be improved for large Re by taking higher-order terms in the expansion, the same is not true for interfacial quantities. Indeed, it is now well established that LWE breaks down at an $\mathcal{O}(1)$ value of the Reynolds number, leading to unacceptable finite-time blowup behavior (e.g., [49,50]).

The IBL approximation was corrected by Ruyer-Quil and Manneville [51–53] who demonstrated that a simple Galerkin projection with just one test function (the self-similar semiparabolic profile assumed by Shkadov) and a weight function the test function itself (the Kármán-Pohlhausen averaging method employed by Shkadov can be viewed as a special weighted residuals technique with a weight function equal to unity), fully corrects the critical Reynolds number and the neutral stability curve close to criticality. Away from criticality, a deviation between the model obtained from the simple Galerkin projection and OS is observed. This deviation is delayed to higher Reynolds numbers by taking into account the second-order viscous diffusive effects. The associated averaging methodology utilizes a high-order weighted residuals approach with polynomial expansions for the velocity field [51–53].

The IBL approximation for free-falling films was extended to falling films in the presence of thermocapillary Marangoni effects induced by heating the substrate either uniformly or nonuniformly by Kalliadasis *et al.* [7,54]. These authors assumed a velocity profile that satisfies the free-surface boundary condition due to the Marangoni effect through a τ method. However, the resulting model still suffers from the main deficiency of IBL for the free-falling film case: namely, a 20% error for the critical Reynolds number. This deficiency was cured for the problem of a uniformly heated wall by Trevelyan and Kalliadasis [8] who combined the τ method of Kalliadasis *et al.* [7,54] with the simple Galerkin projection for the free-falling film employed by Ruyer-Quil and Manneville (which corrects the critical Reynolds number of the IBL approach), appropriately modified for the problem of a uniformly heated wall. The more recent studies by Ruyer-Quil *et al.* [9] and Scheid *et al.* [10] took into account the second-order diffusive terms of the momentum and energy equations and established agreement with OS for a large region of Reynolds numbers (up to $\sim$100). The procedure followed is effectively an extension of the methodology employed by Ruyer-Quil and Manneville to heated falling films and is based on a high-order weighted residuals approach with polynomial expansions for both the velocity and temperature fields.

Here we adapt the study by Trevelyan and Kalliadasis [8] on heated films to falling films in the presence of surfactant. Our starting point is the projection of the velocity field onto the set of polynomial test functions,

$$u = \sum_{i=1}^{N} a_i(x,t)\,\eta^i, \tag{37}$$

where $\eta = y/h(x,t)$ a similarity variable and the amplitudes a_i have to be determined. The corresponding approximation for v is then obtained from Eqs. (31a) and (32). The expansion in (37) satisfies trivially the no-slip boundary condition in (32). We also require that the integral of this expansion with respect to y (or the similarity variable η) gives the flow rate q in the streamwise direction and also satisfies the interfacial boundary condition due to the Marangoni effect in (33). These give

$$\frac{a_1}{2} + \frac{a_2}{3} = \frac{q}{h} - \sum_{i=3}^{N} \frac{a_i}{i+1} \tag{38}$$

and

$$a_1 + 2a_2 = -2\epsilon \mathrm{Ma} h \Gamma_x - \sum_{i=3}^{N} i a_i, \tag{39}$$

which can be solved for a_1 and a_2, which in turn are substituted into (37) to yield

$$u = u^{(0)} + \epsilon \mathrm{Ma} h \Gamma_x \left(\eta - \frac{3}{2}\eta^2 \right) + \sum_{i=2}^{N-1} a_{i+1} \phi_i(\eta), \tag{40a}$$

where

$$u^{(0)} = 3\frac{q}{h}\phi_1(\eta) \equiv 3\frac{q}{h}\left(\eta - \frac{1}{2}\eta^2 \right) \tag{40b}$$

is the self-similar semiparabolic profile for the free-falling film introduced by Shkadov [48] and, for $i=2,3,4,\ldots,N-1$,

$$\phi_i(\eta) = \left(\frac{i+1}{2} - \frac{3}{i+2} \right)\eta + \frac{3}{4}\left(\frac{2}{i+2} - 3(i+1) \right)\eta^2 + \eta^{i+1}. \tag{40c}$$

Hence, by eliminating the amplitudes a_1 and a_2 we have introduced explicitly into the problem the streamwise flow-rate q and we have satisfied the tangential stress boundary condition. As a consequence, we have reduced the number of amplitudes by 1, with q and a_i, $i=3,4,5,\ldots,N$, the amplitudes for the new set of test functions. In effect the elimination of a_1 and a_2 "homogenizes" the tangential stress boundary condition and is equivalent to a tau method. Alternatively, this approach can be viewed as a projection of the function

$$u' \equiv u - \epsilon \mathrm{Ma} h \Gamma_x \left(\eta - \frac{3}{2}\eta^2 \right) \tag{41a}$$

onto the new set of test functions $\phi_i(\eta)$, $i=1,2,3,\ldots,N-1$,

$$u' = \sum_{i=1}^{N-1} a_i' \phi_i(\eta), \tag{41b}$$

where

$$a_1' = \frac{3q}{h} \quad \text{and} \quad a_i' = a_{i+1}, \quad i = 2,3,\ldots,N-1, \tag{41c}$$

so that the tangential stress boundary condition is homogenized.

In general, N must be sufficiently large to achieve convergence; however, we shall demonstrate that, much like the heated falling film problem considered by Trevelyan and Kalliadasis [8], a simple Galerkin projection with just the test function ϕ_1 is sufficient to resolve correctly the behavior close to criticality and describe satisfactorily the nonlinear regime. We shall then truncate the projection in (41) after the first term,

$$u = u^{(0)} + \epsilon \mathrm{Ma} h \Gamma_x \left(\eta - \frac{3}{2}\eta^2 \right), \tag{42}$$

which is the simplest possible velocity profile that satisfies all boundary conditions, and its integral with respect to y (or the similarity variable η) gives the streamwise flow rate q. We also assume that $\epsilon \mathrm{Ma} \ll 1$. Equation (42) then implies that the velocity profile is mainly determined from the balance between the streamwise gravitational component and viscosity and that in the presence of the Marangoni effect the flow is still close to the Nusselt flat-film solution.

The introduction of the profile (42) into the streamwise momentum equation (31b) yields the following residual:

$$\mathcal{R} = \epsilon\,\mathrm{Re}(u_t^{(0)} + u^{(0)}u_x^{(0)} + v^{(0)}u_y^{(0)}) + 2\epsilon h_x \cot\theta - 2\epsilon^3 \mathrm{We} h_{xxx} - u_{yy} - 2, \tag{43}$$

where $v^{(0)} = -\int_0^y u_x^{(0)} dy'$. Note that the Marangoni term in (42) produces terms of $\mathcal{O}(\epsilon^2 \mathrm{MaRe})$ in the inertia terms of the streamwise momentum equation (31b). With $\epsilon \mathrm{Ma} \ll 1$, these terms are neglected compared to the $\mathcal{O}(\epsilon \mathrm{Re})$ terms of the residual (43). However, the Marangoni term in (42) contributes to the viscous diffusion term u_{yy}. In order to neglect then the Marangoni contribution of $\mathcal{O}(\epsilon^2 \mathrm{MaRe})$ in the inertia terms of (31b) compared to the Marangoni contribution of $\mathcal{O}(\epsilon \mathrm{Ma})$ in u_{yy}, we must have $\epsilon \mathrm{Re} \ll 1$. Hence, the order of magnitude assignments in Sec V A, $\epsilon \mathrm{Ma}, \epsilon \mathrm{Re}$ at most of $\mathcal{O}(1)$, are now replaced by $\epsilon \mathrm{Ma}, \epsilon \mathrm{Re} \ll 1$, which shrinks the ranges of Ma, Re (however, Ma, Re can still be large). The remaining orders of magnitude estimates in Sec. V A remain unaltered.

The momentum residual in (43) is then made small by demanding it to be orthogonal to the weight function w_1 which provides a constraint on q and thus a closure for the system,

$$\langle \mathcal{R}, w_1 \rangle = 0, \tag{44}$$

where the inner product is defined as $\langle f,g \rangle = \int_0^1 fg\, d\eta$ for any two functions f and g with appropriate boundary conditions. Specifying the weight function fixes the particular weighted residual method being used. In the case of the Galerkin method, $w_1 \equiv \phi_1$, which after integrations by parts, utilizing the Leibnitz rule, the continuity equation (31a), the no-slip boundary condition (32), and the kinematic boundary condition (33a) yields a nonlinear partial differential equation for q. This equation is complemented by the kinematic boundary

condition (33a), which by integrating the continuity equation (31a) across the film can be written as $h_t+q_x=0$. We also have the concentration equation in (34) with u simply evaluated from (42). As with LWE, the long-wave parameter ϵ is scaled away by reverting back to the original time and space variables—i.e., $x\to\epsilon x$ and $t\to\epsilon t$—which yields the following equations:

$$h_t + q_x = 0, \tag{45a}$$

$$\frac{6}{5}\mathrm{Re}\left(q_t + \frac{17}{7}\frac{qq_x}{h} - \frac{9}{7}\frac{q^2h_x}{h^2}\right) + \frac{3q}{h^2} = 2h - 2hh_x\cot\theta + 2\mathrm{We}hh_{xxx} - 3\mathrm{Ma}\Gamma_x, \tag{45b}$$

$$\Gamma_t + \left[\left(\frac{3q}{2h} - \frac{\mathrm{Ma}}{2}h\Gamma_x\right)\Gamma\right]_x = \frac{1}{\mathrm{Pe_s}}\Gamma_{xx}, \tag{45c}$$

referred to hereafter as the "weighted-integral-boundary-layer" (WIBL) approximation. As its starting point is the first-order boundary-layer equations, this approximation is also first order with respect to the long-wave parameter ϵ.

We now demonstrate that a model very close to the LWE equations in (35) can be obtained from an appropriate expansion of the WIBL system in (45). For this purpose we assign the same order of magnitude for the parameters Re, We, Ma, and $\mathrm{Pe_s}$ as in LWE. Let us now expand q as $q=q_0+q_1+\cdots$, where q_1 is formally of $\mathcal{O}(\epsilon)$ [ϵ needs to be reintroduced in (45)]. We then obtain, from (45),

$$q_0 = \frac{2}{3}h^3 \tag{46a}$$

and

$$q_1 = \frac{8}{15}\mathrm{Re}\,h^6h_x - \frac{2}{3}h^3h_x\cot\theta + \frac{2}{3}\mathrm{We}h^3h_{xxx} - \mathrm{Ma}h^2\Gamma_x. \tag{46b}$$

Equations (45a) and (45c) then with $q=q_0+q_1$ yield Eqs. (35), but with a 4/5 instead of 5/6 in front of the Re term in the concentration equation—i.e., a 4% error. Alternatively, q can be obtained from the iterative scheme

$$\frac{6}{5}\mathrm{Re}\left(q_t^n + \frac{17}{7}\frac{q^nq_x^n}{h} - \frac{9}{7}\frac{(q^n)^2h_x}{h^2}\right) + \frac{3q^{n+1}}{h^2} = 2h - 2hh_x\cot\theta + 2\mathrm{We}hh_{xxx} - 3\mathrm{Ma}\Gamma_x, \quad n=0,1,2,\ldots, \tag{47}$$

where $q^0=q_0=2h^3/3$ and $q_t^0=2h^2h_t=-4h^4h_x$ as obtained from (45a) with $q=q^0$. A single iteration then with $n=0$ gives

$$q^1 = q_0 + q_1 = \frac{2}{3}h^3 + \frac{8}{15}\mathrm{Re}\,h^6h_x - \frac{2}{3}h^3h_x\cot\theta + \frac{2}{3}\mathrm{We}h^3h_{xxx} - \mathrm{Ma}h^2\Gamma_x. \tag{48}$$

Hence the WIBL approximation is compatible with the LWE model, and not surprisingly, as we shall demonstrate shortly, it yields the same Kapitza and concentration modes as the LWE model for small k [up to and including $\mathcal{O}(k^3)$] even though there is a slightly different factor in the concentration equation. This difference is due to the small number of test functions used in the derivation of the WIBL model. As a matter of fact, this difference can be cured by projecting the boundary-layer equations onto a larger set of test functions—i.e., including polynomials of higher order [more precisely, the $\mathcal{O}(\epsilon)$ term for u obtained from the boundary-layer equations involves polynomials of order 4]; however, this will increase both the complexity and dimensionality of the final WIBL equations.

A linear stability now of the steady state $[h,q,\Gamma]=[1,2/3,1]$ with perturbations of the form $\exp(\lambda t+ikx)$ yields three roots for λ, which when expanded for small k become

$$\lambda^1(k) = -2ik + \left(\frac{8}{15}\mathrm{Re} - \frac{2}{3}\cot\theta - 2\mathrm{Ma}\right)k^2 + \left(\frac{7}{30}\mathrm{Re} - \frac{1}{3}\cot\theta + \frac{2}{\mathrm{Pe_s}}\right)\mathrm{Ma}ik^3 + \mathcal{O}(k^4), \tag{49a}$$

$$\lambda^2(k) = -ik - \frac{1}{\mathrm{Pe_s}}k^2 - \left(\frac{7}{30}\mathrm{Re} - \frac{1}{3}\cot\theta + \frac{2}{\mathrm{Pe_s}}\right)\mathrm{Ma}ik^3 + \mathcal{O}(k^4), \tag{49b}$$

$$\lambda^3(k) = -\frac{5}{2\,\mathrm{Re}} + \frac{8}{21}ik + \left(-\frac{8}{15}\mathrm{Re} + \frac{2}{3}\cot\theta + \frac{3}{2}\mathrm{Ma}\right)k^2 + \mathcal{O}(k^3). \tag{49c}$$

The first two modes are identical to those obtained from the LWE model in (36)—not surprising as LWE, albeit with a slightly different numerical factor in the concentration equation, is obtained from the WIBL approximation via an appropriate expansion. However, the WIBL approximation recovers the least stable shear mode with $n=1$ in (23c) obtained from OS, but with a slightly different $\mathcal{O}(1)$ term: 2.5 for the coefficient of 1/Re instead of $\pi^2/4\simeq 2.46$ or $\sim 1\%$ error. Hence, at least as far as the linear instability threshold of the base flow is concerned, the WIBL model is more accurate than the LWE one. Unlike OS, however, it has a finite number of modes due to its polynomial dispersion relation as a result of the projection of the original equations onto a finite number of test functions (one to be precise). Clearly increasing the number of test functions in the projection for the velocity field would increase the number of shear modes while the coefficient of 1/Re would progressively approach its exact value of $\pi^2/4$.

Figure 4 illustrates typical neutral stability curves obtained from OS, LWE, and WIBL. These curves are the locus of the cutoff wave number k at which $\lambda_R^1=0$; hence, in addition to the curves shown in the figure, $k=0$ is also a neutral curve. Note that for the LWE model, only one of the neutral stability curves is plotted, since for some values of the parameters, both the LWE Kapitza and concentration modes exhibit unstable wave numbers. The concentration mode, however, was only destabilized away from criticality; e.g.,

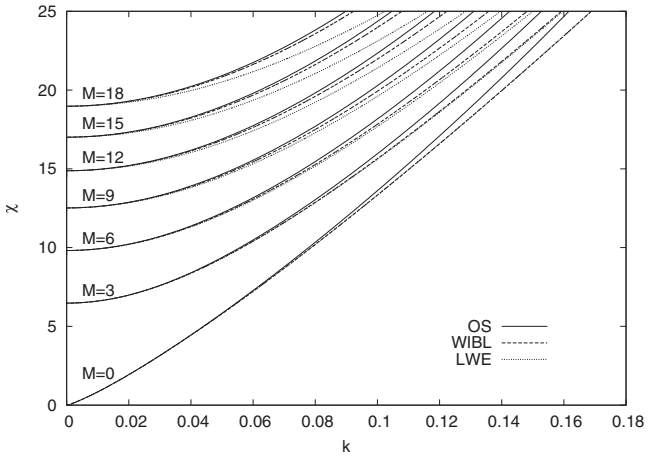

FIG. 4. Neutral stability curves for several values of the Marangoni number (M ranging from 0 to 18 in steps of 3 from bottom to top). The solid lines refer to the Orr-Sommerfeld equations, the dashed ones to the WIBL model, and the dotted ones to the LWE model. The unstable area is located above the curves. The values of the remaining parameters are the same with those in Fig. 2. The neutral curves have also a second branch which is simply the one with $k=0$ for all χ. Note that for the LWE model, only one of the neutral stability curves is plotted, since for some values of the parameters, both the LWE Kapitza and concentration modes exhibit regions with unstable wave numbers.

for $\chi=25$ and $M=18$ there is a concentration mode instability region with a "tongue-type" shape starting from $k\simeq 0.1$ and without any overlap with the instability region associated with the Kapitza mode. This is a spurious effect owing to the fact that the LWE model is not able to capture accurately the behavior far from criticality (see also our discussion in Sec. V C). Indeed, both the OS and WIBL models predict that the concentration mode is always stable, as it should be given its "diffusional" character as we pointed out in Sec. IV B.

Figure 4 indicates that by increasing M the region of instability shrinks, thus confirming the stabilizing role of the surfactant on the steady state: not only the critical Reynolds number increases, but also, for a given Re, the range of unstable wave numbers is shortened. It also shows that close to criticality both LWE and WIBL models predict accurately the neutral curves (as we have already pointed out both models predict accurately the neighborhood of the linear instability threshold) and the critical values of χ for which the destabilization occurs (values of χ for $k=0$) agree with Eq. (24). The figure also shows clearly the overall superiority of the WIBL model compared to the LWE model for $M\neq 0$. For $M\neq 0$, the WIBL model also performs better for k way outside the region shown in the figure. As was emphasized in Sec. V C the LWE neutral curve can be improved by including higher-order terms in the expansion. As was also discussed in the same subsection, the WIBL neutral curve can be improved by taking into account the second-order diffusive effects by analogy with both the free- and heated-falling problems.

VI. SOLITARY WAVES

We now seek traveling wave solutions propagating at constant speed c. We introduce the moving coordinate transformation $z=x-ct$ into the LWE model (35) and WIBL model (45) with $\partial/\partial t=-c\partial/\partial z$ for the waves to be stationary in the moving frame. The equations obtained from the LWE model then in the moving frame can be integrated once, and we fix the integration constants by demanding that $[h,\Gamma]\to[1,1]$ as $z\to\pm\infty$ appropriate for solitary wave solutions. This gives

$$\mathrm{We}h^3h''' - \frac{3}{2}c(h-1) + h^3 - 1 - \mathrm{cotan}\,\theta h^3h' + \frac{4}{5}\,\mathrm{Re}\,h^6h' - \frac{3}{2}\mathrm{Ma}h^2\Gamma' = 0, \tag{50a}$$

$$\mathrm{We}h^2\Gamma h''' - c(\Gamma-1) + h^2\Gamma - 1 - \mathrm{cotan}\,\theta h^2\Gamma h' + \frac{5}{6}\,\mathrm{Re}\,h^5\Gamma h' - 2\mathrm{Ma}h\Gamma\Gamma' - \frac{1}{\mathrm{Pe_s}}\Gamma' = 0, \tag{50b}$$

where the primes denote differentiation with respect to z. These equations together with the boundary conditions $[h,\Gamma]\to[1,1]$ as $z\to\pm\infty$ and all the derivatives of h,Γ approaching zero as $z\to\pm\infty$ define a nonlinear eigenvalue problem for the speed c of the solitary waves. Similarly, introducing the moving coordinate into (45a) yields $-ch_z+q_z=0$, which can be integrated once, and we fix the integration constant by demanding $[h,q]\to[1,2/3]$ (these values are obtained from the Nusselt base state). This gives a relation between the flow rate and film thickness:

$$q = \frac{2}{3} + c(h-1). \tag{51a}$$

We also introduce the moving coordinate into (45b) and (45c), we integrate the resulting concentration equation once, and we fix the integration constant from $\Gamma\to 1$ as $z\to\pm\infty$:

$$\mathrm{We}hh''' = \frac{3}{5}\,\mathrm{Re}\left(-c^2 + \frac{17}{7}\frac{qc}{h} - \frac{9}{7}\frac{q^2}{h^2}\right)h' + \frac{3q}{2h^2} - h + \mathrm{cotan}\,\theta hh' + \frac{3}{2}\mathrm{Ma}\Gamma', \tag{51b}$$

$$\left(\mathrm{Ma}\frac{h\Gamma}{2} + \frac{1}{\mathrm{Pe_s}}\right)\Gamma' = c - 1 + \left(\frac{3q}{2h} - c\right)\Gamma. \tag{51c}$$

Again, these equations together with the boundary conditions $[h,\Gamma]\to[1,1]$ as $z\to\pm\infty$ and all the derivatives of h,Γ approaching zero as $z\to\pm\infty$ define a nonlinear eigenvalue problem for the speed c of the solitary waves.

Our aim here is to construct the solitary wave solutions of the LWE and WIBL models. We restrict our attention to single-hump solitary waves. They correspond to "principal homoclinic orbits" of the dynamical systems corresponding to the traveling wave models. We shall demonstrate in the next section that these solutions are the main feature of the nonlinear behavior of the system following the linear destabilization of the base flow. We compute them using the continuation software AUTO97 [44]. For this purpose Eqs. (50)

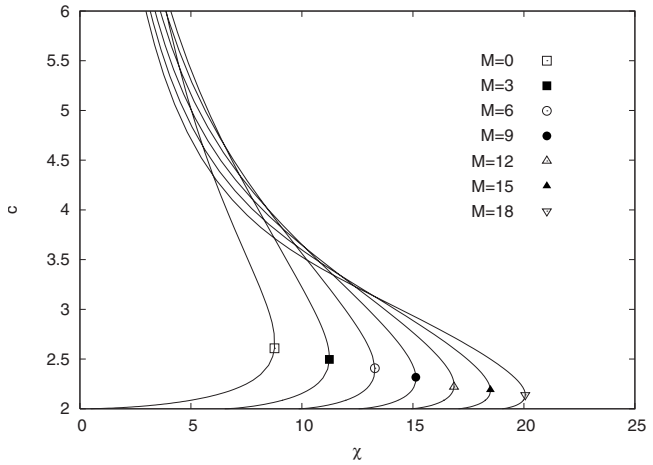

FIG. 5. LWE solitary wave bifurcation diagrams for the speed c as a function of the modified Reynolds number χ. The modified Marangoni number M ranges from 0 to 18 in steps of 3 from left to right. The remaining dimensionless groups are the same as in Fig. 2.

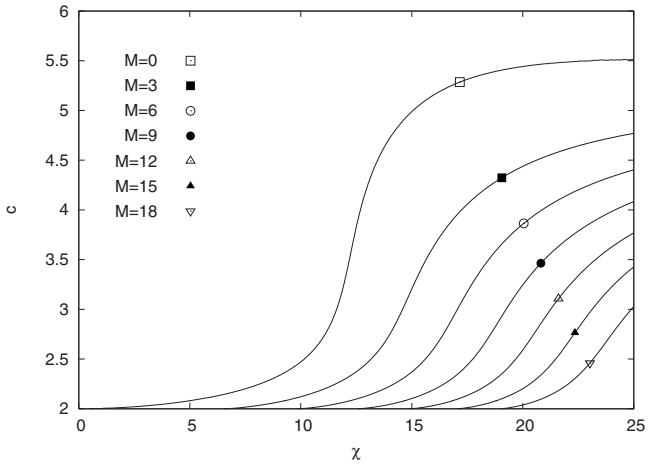

FIG. 6. WIBL solitary wave bifurcation diagrams for the speed c as a function of the modified Reynolds number χ. The modified Marangoni number M ranges from 0 to 18 in steps of 3 from left to right. The remaining dimensionless groups are the same as in Fig. 2.

and (51) are converted into fourth-order dynamical systems for the vector $[h,h',h'',\Gamma]$. We impose periodic boundary conditions in a domain of size L—i.e., $h=1$, $\Gamma=1$, $h'=0$, and $\Gamma'=0$ (a total of five conditions)—and not all of them at $x=0$ or $x=L$. The computation of the solution branches consists of two steps: obtaining a good starting solution for a given χ, e.g., close to its critical value and then continuing the solution with χ as continuation parameter. The initial condition for the starting solution is a small-amplitude sine with wave number the maximum growing one as predicted by the linear stability analysis. For the LWE model we then continue this solution with L as a continuation parameter while χ and the remaining parameters remain fixed (for the WIBL model this first step is in general much more involved and might require simultaneous continuation with respect to L and three to four other parameters). This continuation process increases L up to a point where at least 70–80% of the domain is flat and there is no significant variation of the solution when L increases further. This then implies that, for the given value of χ, we are on the branch of homoclinic solutions. We then fix L and continue the solution by using χ as a continuation parameter.

Figure 5 depicts typical bifurcation diagrams for the LWE solitary wave speed c as a function of χ for different values of M. As we focus on the coupling between the flow and the surfactant, only χ and M are varied in our computations. Close to criticality, traveling waves only exist if the flow, through χ, is strong enough. The solution branches then start from the threshold value of χ given in Eq. (24). Away from the threshold, the branches exhibit turning points at certain values of χ which depend on M and branch multiplicity with two branches, a lower one and an upper one. Clearly the upper branch is unrealistic as it predicts solitary waves with infinite speed as $\chi\to 0$. Similar LWE bifurcation diagrams are also found for the free-falling problem as well as the falling film heated from below [8] and the falling film in the presence of exothermic chemical reactions [13–15]. For the free-falling film problem, Pumir *et al.* [49] demonstrated for the first time that the LWE model exhibits finite-time blowup behavior for a sufficiently large set of smooth initial conditions when this equation is integrated in time for Reynolds numbers larger than those corresponding to the turning points. Clearly, this unrealistic behavior is related to the model's nonexistence of solitary waves. The connection between the absence of solitary wave solutions and finite-time blowup was recently investigated by Scheid *et al.* [50]. The blowup behavior marks the failure of the LWE model to correctly describe nonlinear waves far from criticality (recall from our previous discussions that the LWE model fully resolves the behavior close to the instability threshold) and cannot be cured by taking more terms in the expansion, although as we emphasized in Sec. V C, this would improve the LWE neutral curve. The same failure occurs for the falling film heated from below and the falling film in the presence of exothermic chemical reactions [8,13–15]. Similarly, in our case time-dependent computations reveal a catastrophic behavior when the LWE model is integrated in regions of the parameter space where solitary waves do not exist.

Figure 6 shows typical bifurcation diagrams for the WIBL solitary wave speed as a function of χ for different values of M. Unlike the LWE model, the WIBL model has no turning points and predicts the continuing existence of solitary pulses for all χ. Similarly, we shall demonstrate in the next section that unlike the LWE model, the WIBL model is quite robust in time-dependent computations without any singularity formation. As χ increases, the wave speed increases, until for sufficiently large χ, the speed (and therefore amplitude) of the solitary pulses seems to asymptote to certain values. These values decrease with increasing M. In fact, for a given χ, increasing M decreases the speed (and therefore amplitude) of the solitary pulses, a manifestation of the stabilizing influence of the surfactant. This is also the case with the lower branches of Fig. 5. Moreover, the lower branches of Fig. 5 are in agreement with the WIBL ones up to approximately the location of the turning points. This should not be surprising since a model very close to the LWE model can be obtained from the WIBL model via an appropriate expansion as we demonstrated in the previous section.

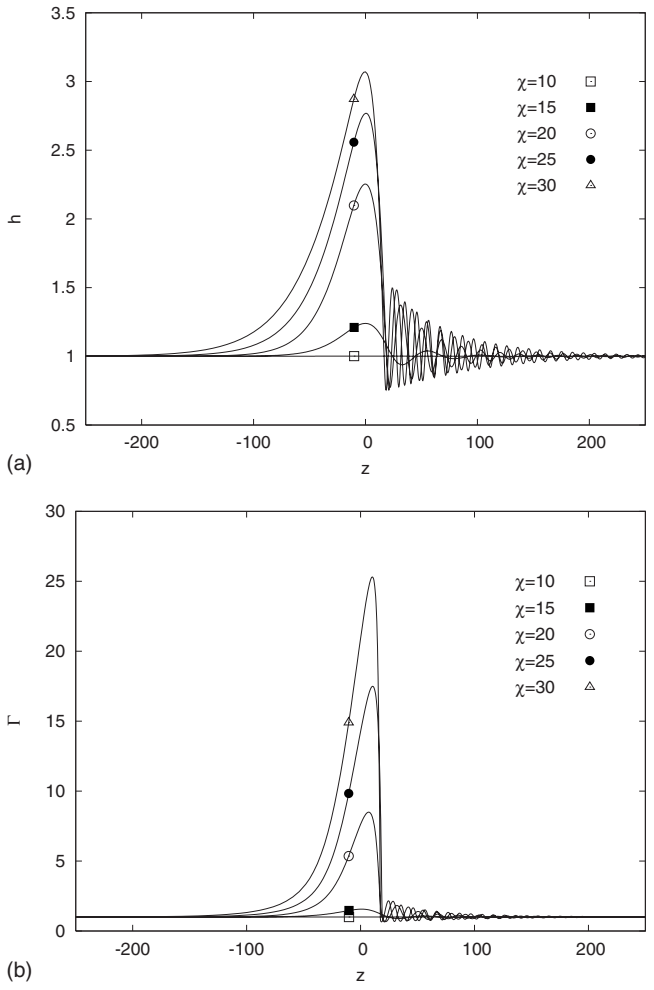

FIG. 7. Solitary pulses for the free surface (a) and surfactant concentration (b) for $M=6$ obtained from the WIBL model in Eq. (51). χ ranges from 10 to 30 in steps of 5 from bottom to top. The values of the remaining parameters are the same with those in Fig. 2.

Figure 7 shows typical solitary wave shapes for both free surface and surfactant concentration. The free-surface solitary pulses are qualitatively similar to the free-falling film solitary pulses and consist of a primary solitary hump connected to the flat film with a gentle slopped back edge region and a steep front edge region followed by a series of small decaying bow waves. The surfactant concentration solitary pulse also has a similar shape. Note that as χ increases the amplitude (and hence speed) of both free-surface and surfactant concentration solitary pulses increases, a signature of the destabilizing role of inertia in the system.

Let us now discuss the physical implications of the bifurcation diagrams in Fig. 6. As with Tables I and II we assume a film of water at 25°. We also assume a modified Reynolds number $\chi=20$ which corresponds to $h_0=0.117$ mm ($q_0=5.9$ mm^2 s^{-1}) and $u_0=0.0757$ m s^{-1}. From Fig. 6, we note that the velocity of the solitary waves decreases from $\sim 5.5u_0$ to $\sim 2u_0$, or from 0.42 m s^{-1} to 0.15 m s^{-1}—i.e., a reduction by a factor of 3 as the surfactant concentration increases from 0 (i.e., $M=0$) to 1.3×10^{-7} mol m^{-2} (i.e., $M=18$). The latter value for the surfactant concentration corresponds to a small uniform surfactant concentration compared to the maximum one—i.e., $\Gamma_0 \sim 0.1\Gamma_\infty$—and can accordingly be easily reached in experiments. However, despite the smallness of Γ_0 compared to Γ_∞, the surfactant effect on the speed and therefore amplitude of solitary waves is significant, as was first emphasized in Sec. II.

Moreover, increasing the Schmidt number to values above 100 in Fig. 6 has a negligible effect on the bifurcation structure and hence speed and amplitude of solitary waves. Indeed, for $M=18$ and $\chi=20$ increasing Sc to 1000, or even 10 000, has practically no effect on the dimensionless velocity $c \simeq 2.038$. As a matter of fact, any $\mathrm{Sc} \gtrsim 100$ gives the same result for c for a given χ. That is because for $\mathrm{Sc} \gtrsim 100$, the surface Péclet number Pe_s is large and we lose the effect of surface diffusion (for $\chi \gtrsim 100$, $\mathrm{Pe}_s \gtrsim 1000$ for $\chi=20$): as emphasized in Sec. V A, when Pe_s is large, convection dominates over surface diffusion and the surfactant travels on the film surface by convection only, not diffusion. Since now, for fixed Γ_∞, M is affected by Γ_0/Γ_∞ only as discussed in Sec. III, it is this ratio that really matters and not the particular surfactant molecule (of course, the underlying basic assumption here is that the surfactant obeys the von Szyszkowski equation). In other words, for $\chi=20$ and fixed Γ_∞, the speed of the solitary pulses is reduced by a factor of 3 independently of the surfactant molecule provided that $\mathrm{Sc} \gtrsim 100$.

We now turn to the structure of the flow field beneath a solitary pulse. In addition to the amplitude and speed of the solitary pulses, the x component of the interfacial velocity at $y=h$, u_s obtained from Eqs. (42) and (51b),

$$u_s = \frac{3c}{2} - \frac{1}{2h}(3c-2) - \frac{\mathrm{Ma}}{2}\Gamma' h, \tag{52}$$

also increases as χ increases, which can lead to a change in the relative magnitude of the wave speed c and interfacial velocity u_s. This might have some dramatic consequences for the surfactant concentration, whose governing equation in the moving frame (51c) can be rewritten as

$$\frac{1}{\mathrm{Pe}_s}\Gamma' = c - 1 + (u_s - c)\Gamma. \tag{53}$$

To illustrate let us assume for simplicity that $\mathrm{Ma}=0$. The value of c as well as u_s [$=u_s(z)$] are then completely determined by Eqs. (51b) and (52)—i.e., without the need of Eq. (51c). At the instability onset the interface is flat and $u_s=1$ due to the choice of the velocity scale (the Nusselt flat-film velocity; see Sec. III). Hence the velocity of the flow near the interface is smaller than the wave velocity, which equals 2; see Fig. 6 (the kinematic wave velocity).

Consider now Eq. (52) with $\mathrm{Ma}=0$. u_s has two terms: $3c/2$ and $(3c-2)/2h$, which are positive since $c>2$. For a fixed χ and therefore c, as the film thickness h increases, the second term decreases and hence u_s increases. This implies that for a given χ the maximum of u_s, $u_{s,\max}$, occurs at the peak of the wave. Now, as χ increases, our computations show that $u_{s,\max}$ increases so that, at some χ, $u_{s,\max}=c$. We now have a recirculation zone: indeed the streamlines in the moving frame correspond to envelopes of the velocity field

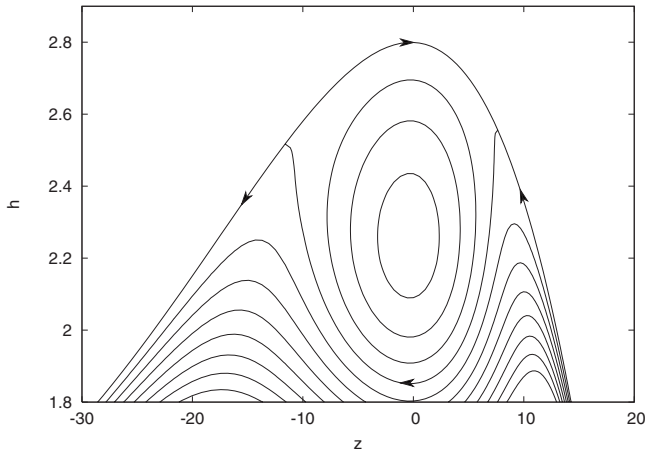

FIG. 8. Streamlines in the moving frame for $\chi=15$ and $M=0.1$. The remaining dimensionless groups are the same with those in Fig. 2. A clockwise recirculation zone is present below the primary solitary hump. The formation of this zone is a consequence of the fact that the velocity of the flow at the surface of the film increases as the wave height increases and eventually it can exceed the velocity of the wave in some areas of the film.

in the moving frame (U,v) with $U=u-c$. Recirculation zones indicate regions where the flow returns with $v=0$ or stagnation points where $U=v=0$. (Note, however, that in the laboratory frame these regions have $u=c\gg v$ so that the condition $u\gg v$ in the laboratory frame necessary for the long-wave assumption still holds.) Since then $u_{s,\max}=c$ implies a recirculation zone and $u_{s,\max}$ occurs at the wave peak, the recirculation zone starts from a single stagnation point right at the top of the wave and then spreads into the wave as χ increases with two stagnation points, one at the front of the wave and another one at its back, while $u_{s,\max}$ becomes larger than c.

Figure 8 shows a recirculation zone beneath the primary solitary hump for $\chi=15$ and $M=0.1$ Recall that for simplicity the above discussion was restricted to the limiting case $M=0$. Nevertheless, this case helped us identify the mechanism of the formation of the recirculation zone. The zone shown in the figure has two stagnation points on either side of the peak. At these stagnation points $u_s=c$, while inside the recirculation zone u_s exceeds c. Due to the particular structure of the free-surface flow field around the front stagnation point, with fluid particles from either side of the stagnation point moving towards it, we expect a significant accumulation of surfactant there with a large value of Γ close to this point, provided that the Péclet number is large—i.e., that the diffusion coefficient of the surfactant is small—which indeed is the case in the figure since $\chi=15$ and $\mathrm{Sc}=100$. In other words, as the wave moves from the left to the right, it continuously sweeps surfactant whose concentration then builds up at the front stagnation point. When the recirculation zone is first born as a single point at the wave peak, Γ has a large value close to this point. However, provided that the surfactant is able to diffuse—i.e., Pe_s is finite—this pileup of surfactant does not lead to a true singularity formation for Γ. On the other hand, when $\mathrm{Pe}_s\to\infty$, Eq. (53) shows that Γ develops a singularity for $u_s=c$. Note that $M\neq 0$ reduces the accumulation of surfactant as shown in Fig. 9. The stabilizing influence of the Marangoni effect on the interface reduces the maximum amplitude of the solitary pulse as shown in Fig. 9(a). Despite the fact that the amplitude change is small and hence the change of u_s-c is small, u_s-c remains close to zero and small changes of this quantity can have a significant effect on Γ (recall, e.g., that when $\mathrm{Pe}_s\to\infty$, u_s-c is responsible for a true singularity for Γ). The result of increasing M is a dramatic reduction of the maximum value of Γ. As a matter of fact, our computations indicate that the Marangoni effect delays the appearance of recirculation zones and hence the appearance of large values of Γ to larger χ. For very large M, this delay can be so significant that recirculation zones do not occur at all (at least in the region of moderate Reynolds numbers considered here) as u_s never reaches c.

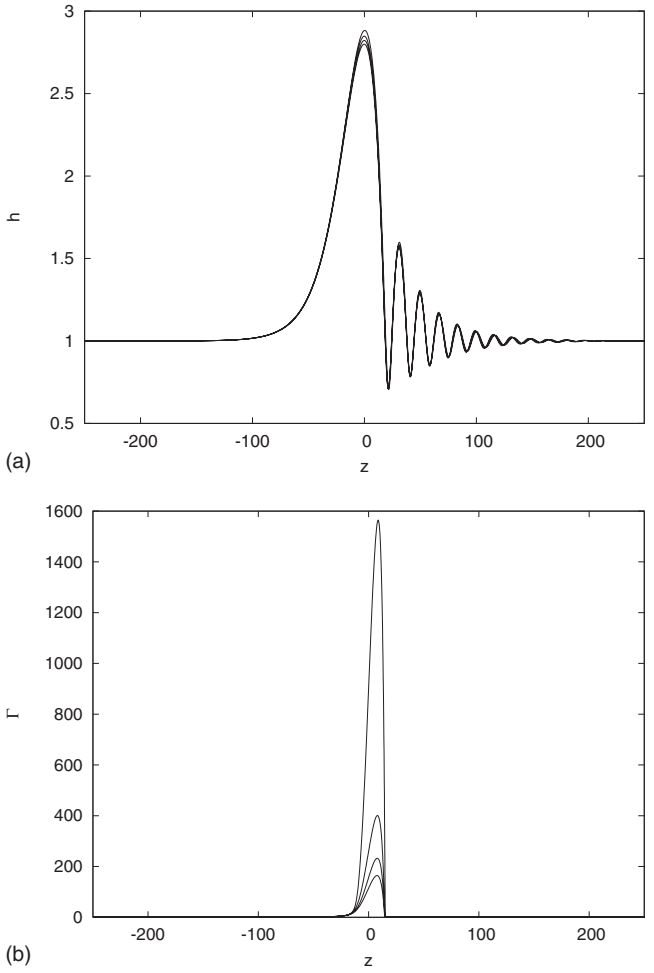

FIG. 9. Solitary pulses for the free surface (a) and surfactant concentration (b) for $\chi=15$ as M increases ($0.01\to 0.10$ in steps of 0.03 from top to bottom). The remaining dimensionless groups are the same as in Fig. 2. The stabilizing influence of the Marangoni stresses reduces the surfactant pile up due to the presence of a recirculation zone beneath the free-surface solitary hump.

Of course, our WIBL model is not applicable when the dimensional concentration Γ is large. Indeed, as was pointed out in Sec. II, when the concentration of surfactant increases to large values the mechanical properties of the interface change drastically: the interface becomes increasingly

"rigid" starting to develop rheological properties and additional effects neglected here such as surface viscosity might have to be added [31]. Further, it is quite likely that when the surfactant piles up at the stagnation point, and since it has nowhere to go, the flow might force it into the liquid, even though it is insoluble, or it might be expelled to the surrounding gas.

However, large dimensionless concentrations do not necessarily correspond to large dimensional ones. Indeed, for the peak value $\Gamma \sim 25$ in Fig. 7, assuming a reference dimensional concentration $\Gamma_0 = (1/25) \times 10^{-6}$ mol m^{-2}, gives a dimensional concentration $\Gamma \sim 10^{-6}$ mol m^{-2}, which is moderate compared to Γ_∞ in Table I, and $M = 5.4$ very close to the value of 6 in the computations of Fig. 7. Hence, the concentrations reported in this figure are not unphysical. Similarly, for the conditions in Fig. 9, the maximum dimensionless concentration of $\Gamma \sim 1600$ gives a dimensional concentration of $\Gamma \sim 1.6 \times 10^{-9}$ mol m^{-2} by assuming $\Gamma_0 \sim 10^{-9}$ mol m^{-2}, a moderate value compared to Γ_∞ in Table I, a small value $M \sim 10^{-2}$. Again the concentration peak is physical, but now the long-wave approximation is violated, unlike Fig. 7. Eventually, for large χ large dimensional concentrations can result.

VII. TIME-DEPENDENT EVOLUTION

The existence of a special class of solutions—namely, solitary waves stationary in a moving frame—raises the question of relevance of these solutions which is related to the way they attract initial conditions. An answer to this question can be given by means of a numerical solution of Eqs. (45) as an initial-value problem. For this purpose we employed a Crank-Nicholson-type implicit scheme with the spatial derivatives approximated by central differences and with dynamic time-step adjustment to monitor the accuracy of the computations. We impose periodic boundary conditions over an extended domain, much larger than the maximum growing wavelength predicted by the linear stability analysis.

Figure 10 depicts the evolution for the free surface and surfactant concentration using as initial condition for the free surface h a Gaussian distribution in the middle of the domain and $[q, \Gamma] = [2/3, 1]$—i.e., their flat-film values. The results are presented in the moving frame with the velocity of the corresponding infinite domain stationary solitary pulse for the free surface and concentration obtained from the traveling wave equations (51) for the same parameter values. The localized initial condition for h through the coupling with the Marangoni effect induces at early times a localized disturbance for Γ. Both h and Γ localized structures then start growing and speeding up until for large times the system evolves into the infinite-domain stationary solitary pulse obtained from the traveling wave equations (51) for the same parameter values and the velocity approaches asymptotically the velocity $c = 2.370\,12$ of the bifurcation diagram in Fig. 6. We also observe a radiation wave packet forming to the back of the solitary pulse, and much like free-falling films, this wave packet will eventually give birth to additional solitary pulses.

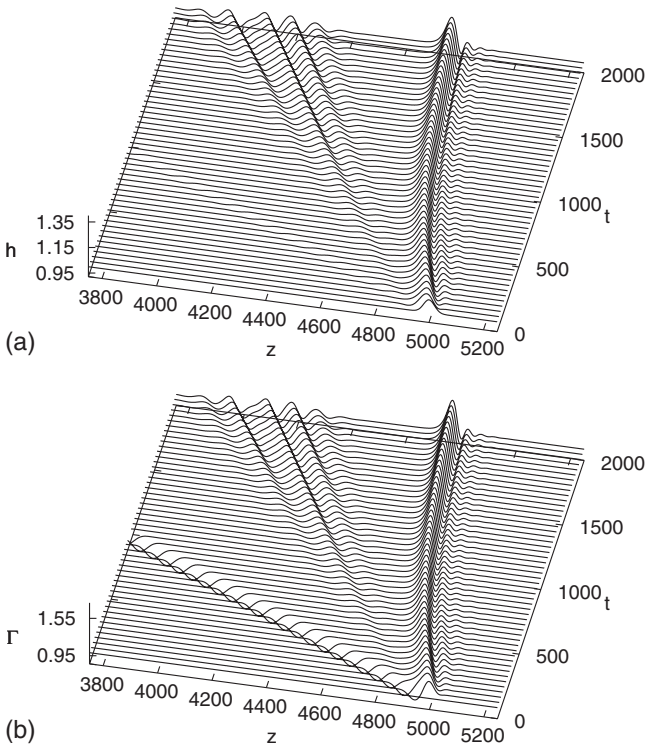

FIG. 10. Time evolution for the free surface height h and surfactant concentration Γ obtained from the WIBL model in (45) for $\chi = 15$, $M = 6$, and the values of the remaining parameters the same with those in Fig. 2. The initial condition is $q = 2/3$, $\Gamma = 1$, and a Gaussian distribution for the free surface in the middle of the domain, $h = 1 + A \exp[-x^2/(2\Sigma)]$, with amplitude $A = 0.1$ and variance $\Sigma = 400$. The domain size is 10 000, and successive curves are separated by $\Delta t = 40$. The results are displayed in the moving frame with velocity $c = 2.37012$, the velocity of the corresponding stationary solitary wave solution for the free surface and concentration obtained from the traveling wave equations (51).

The formation of the solitary pulse in Fig. 10 is driven by the Kapitza interfacial mode of instability analyzed in Sec. IV B. Figure 10(b) also reveals a small amplitude "dip" emanating from the middle of the domain at small times and traveling backwards in the moving frame. In the laboratory frame the speed of this structure is ~ 1 and corresponds precisely to the stable concentration mode analyzed in Sec. IV B. Since the value of Pe_s in these computations is large, this concentration wave decays very slowly as it is advected by the flow.

Figure 11 shows the evolution for the free surface and surfactant concentration using as initial condition for h random noise and $[q, \Gamma] = [2/3, 1]$. The results are presented in the moving frame with the kinematic wave velocity $c = 2$. The large-time evolution is characterized by trains of solitonlike coherent structures of almost the same amplitude and which interact indefinitely with each other. These coherent structures possess a gently slopping back edge and a steep front edge preceded by some small bow waves and are reminiscent of the infinite-domain stationary solitary pulses obtained in the bifurcation diagram of Fig. 6.

These computations show the relevance of the solutions obtained in Sec. VI in the nonlinear regime following the

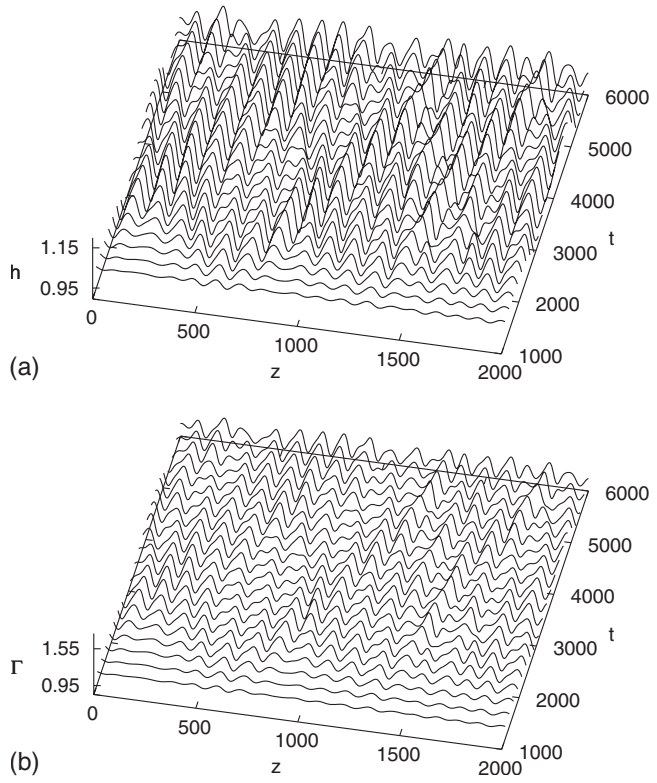

FIG. 11. Time evolution for the free surface height h and surfactant concentration Γ obtained from the WIBL model for $\chi=15$, $M=6$, and the values of the remaining parameters the same with those in Fig. 2. The initial condition is $q=2/3$, $\Gamma=1$, and random noise of maximum amplitude 0.01 for h. The domain size is 2000. The results are displayed in a moving frame with the linear kinematic wave velocity $c=2$.

destabilization of the steady state due to the Kapitza mode. Moreover, for the parameter values in Figs. 10 and 11, the LWE prototype does not have any stationary solitary wave solutions (Fig. 5) and in fact it blows up in finite time. The WIBL prototype, on the other hand, is always quite robust and does not exhibit any singularity formation.

VIII. CONCLUSIONS

We investigated the dynamics of a film falling down a planar substrate in the presence of insoluble surfactant on its free surface. We examined the Orr-Sommerfeld eigenvalue problem of the full Navier-Stokes and concentration equations and associated wall and free-surface boundary conditions via a small-wave-number expansion and a full numerical solution. This allowed us to assess the linear stability characteristics of the system: there are three types of modes: the Kapitza interfacial mode, which is responsible for the destabilization of the free surface; a concentration mode, which is neutrally stable for large surface Péclet numbers; and the shear modes, which can only be destabilized for very large Reynolds numbers. The role of the Marangoni effect in the linear regime is to dampen the Kapitza mode and reduce the critical Reynolds number for the instability onset.

Subsequently, we developed two reduced models to account for the description of the nonlinear regime following the destabilization of the steady state due to the Kapitza mode. The first one is based on the classical long-wave expansion and the second one on a weighted residuals approach. Both models predict accurately the critical Reynolds number for the instability onset, and their neutral stability curves are in good agreement with those obtained from the Orr-Sommerfeld analysis (with the curves of the second model being in better agreement with Orr-Sommerfeld than those of the first one).

We then focused on the nonlinear regime. In particular, we constructed bifurcation diagrams for the speed of single-hump solitary waves for the free surface and concentration as a function of the Reynolds number. The bifurcation diagrams of the first model were found to be unrealistic with turning points and branch multiplicity at certain Reynolds numbers. As a consequence of this, the model exhibits finite-time blowup behavior in the region where solitary waves do not exist, a sign of its inability to correctly describe nonlinear waves far from criticality: it is only valid close to the instability threshold. On the other hand, the solitary wave solution branches of the second model have no turning points and show the continuing existence of solitary waves for all Reynolds numbers. In fact, this prototype is found to be robust in time-dependent computations without any singularity formation, which allows a quantitative description of the role of the surfactant in the nonlinear regime. These computations also reveal that the large-time behavior is characterized by wave structures each of which resembles the infinite-domain stationary solitary pulses.

The main effect of the surfactant in the nonlinear regime is to dampen the free-surface solitary waves. In contrast, the flow tends to induce accumulation of surfactant at the front stagnation point of a free-surface solitary pulse for sufficiently large Reynolds numbers. This could have a dramatic effect on surfactant concentration causing large concentration values close to the front stagnation point of a recirculation zone below the primary solitary hump, especially for small Marangoni numbers. Such large values are unrealistic and can be prevented by increasing the Marangoni number, which can cause a significant reduction of the maximum of the surfactant concentration, while large values of the Marangoni number can even suppress this phenomenon all together as they prevent the formation of recirculation zones.

ACKNOWLEDGMENTS

We are grateful to P.M.J. Trevelyan, C. Ruyer-Quil, and B. Scheid for useful comments and discussions. We acknowledge financial support from the Engineering and Physical Sciences Research Council of the UK (EPSRC) through Grant No. GR/S79121. S.K. acknowledges financial support from the EPSRC through Grant No. GR/S49520.

[1] P. Kapitza, Zh. Eksp. Teor. Fiz. **18**, 3 (1948).
[2] P. L. Kapitza and S. P. Kapitza, Zh. Eksp. Teor. Fiz. **19**, 105 (1949).
[3] H.-C. Chang, Annu. Rev. Fluid Mech. **26**, 103 (1994).
[4] H.-C. Chang and E. A. Demekhin, *Complex Wave Dynamics on Thin Films* (Elsevier, Amsterdam, 2002).
[5] D. Goussis and R. Kelly, J. Fluid Mech. **223**, 24 (1991).
[6] S. Joo, S. Davis, and S. Bankoff, J. Fluid Mech. **230**, 117 (1991).
[7] S. Kalliadasis, E. A. Demekhin, C. Ruyer-Quil, and M. G. Velarde, J. Fluid Mech. **492**, 303 (2003).
[8] P. M. J. Trevelyan and S. Kalliadasis, J. Eng. Math. **50**, 177 (2004).
[9] C. Ruyer-Quil, B. Scheid, S. Kalliadasis, M. G. Velarde, and R. Kh. Zeytounian, J. Fluid Mech. **538**, 199 (2005).
[10] B. Scheid, C. Ruyer-Quil, S. Kalliadasis, M. G. Velarde, and R. Kh. Zeytounian, J. Fluid Mech. **538**, 223 (2005).
[11] B. Scheid, A. Oron, P. Colinet, U. Thiele, and J. C. Legros, Phys. Fluids **14**, 4130 (2002).
[12] E. A. Demekhin, S. Kalliadasis, and M. G. Velarde, Phys. Fluids **18**, 042111 (2006).
[13] P. M. J. Trevelyan, S. Kalliadasis, J. H. Merkin, and S. K. Scott, Phys. Fluids **14**, 2402 (2002).
[14] P. M. J. Trevelyan and S. Kalliadasis, Phys. Fluids **16**, 3191 (2004).
[15] P. M. J. Trevelyan and S. Kalliadasis, Phys. Fluids **16**, 3209 (2004).
[16] W. Ji and F. Setterwall, J. Fluid Mech. **278**, 297 (1994).
[17] V. Ya. Shkadov, M. G. Velarde, and V. P. Shkadova, Phys. Rev. E **69**, 056310 (2004).
[18] M. Blyth and C. Pozrikidis, J. Fluid Mech. **521**, 241 (2004).
[19] C. Pozrikidis, J. Fluid Mech. **496**, 105 (2003).
[20] H. Luo and C. Pozrikidis, Acta Mech. **188**, 209 (2007).
[21] H. Luo and C. Pozrikidis, Phys. Fluids **18**, 078107 (2006).
[22] A. Pereira, P. M. J. Trevelyan, U. Thiele, and S. Kalliadasis, Phys. Fluids **19**, 112102 (2007).
[23] A. Pereira and S. Kalliadasis, Eur. Phys. J.: Appl. Phys. (to be published).
[24] H. A. Stone, Phys. Fluids A **2**, 111 (1990).
[25] P. Cermelli, E. Fried, and M. Gurtin, J. Fluid Mech. **544**, 339 (2005).
[26] A. Oron, S. H. Davis, and S. G. Bankoff, Rev. Mod. Phys. **69**, 931 (1997).
[27] S. Kalliadasis and U. Thiele, *Thin Films of Soft Matter*, CISM International Centre for Mechanical Sciences (Springer-Wien, New York, 2007).
[28] D. P. Gaver III and J. B. Grotberg, J. Fluid Mech. **235**, 399 (1992).
[29] A. J. Prosser and E. I. Franses, Colloids Surf., A **178**, 1 (2001).
[30] C. D. Eggleton, Y. P. Pawar, and K. J. Stebe, J. Fluid Mech. **385**, 79 (1999).
[31] A. Nepomnyashchy, M. G. Velarde, and P. Colinet, *Interfacial Phenomena and Convection* (Chapman & Hall/CRC, London, 2002).
[32] N. R. Gupta, A. Nadim, H. Haj-Hariri, and A. Borhan, J. Colloid Interface Sci. **252**, 236 (2002).
[33] J. Li, Eur. J. Mech. B/Fluids **25**, 59 (2006).
[34] I. B. Bazhlekov, P. D. Anderson, and H. E. H. Meijer, J. Colloid Interface Sci. **298**, 369 (2006).
[35] S. V. Alekseenko, V. E. Nakoryakov, and B. G. Pokusaev, *Wave Flow in Liquid Films*, 3rd ed. (Begell House, New York, 1994).
[36] V. M. Starov, A. de Ryck, and M. G. Velarde, J. Colloid Interface Sci. **190**, 104 (1997).
[37] C. L. Yaws, *Chemical Properties Handbook: Physical, Thermodynamic, Environmental, Transport and Safety Properties of Organic and Inorganic Chemicals* (McGraw-Hill, New York, 1998).
[38] I. M. Umlong and K. Ismail, J. Colloid Interface Sci. **291**, 529 (2005).
[39] J. M. Floryan, S. H. Davis, and R. E. Kelly, Phys. Fluids **30**, 983 (1987).
[40] T. B. Benjamin, J. Fluid Mech. **2**, 554 (1957).
[41] C.-S. Yih, Phys. Fluids **6**, 321 (1963).
[42] T. Benjamin, Arch. Mech. Stosow. **16**, 615 (1964).
[43] S. Whitaker, Ind. Eng. Chem. Fundam. **3**, 132 (1964).
[44] E. Doedel, A. Champneys, T. Fairfrieve, Y. Kuznetsov, B. Sandstede, and X. Wang, ftp.concordia.ca/pub/doedel/auto
[45] H. B. Keller in *Applications of Bifurcation Theory*, edited by P. H. Rabinowitz (Academic, New York, 1977), pp. 359–384.
[46] E. A. Demekhin and V. Ya. Shkadov, Izv. Akad. Nauk SSSR, Mekh. Zhidk. Gaza **5**, 21 (1984).
[47] H. Schlichting, *Boundary-Layer Theory* (McGraw-Hill, New York, 1968).
[48] V. Ya. Shkadov, Izv. Akad. Nauk SSSR, Mekh. Zhidk. Gaza **1**, 43 (1967); English translation in *Fluid Dynamics* (Faraday Press, New York, 1970), Vol. 2, pp. 29–34.
[49] A. Pumir, P. Manneville, and Y. Pomeau, J. Fluid Mech. **135**, 27 (1983).
[50] B. Scheid, C. Ruyer-Quil, U. Thiele, O. A. Kabov, J. C. Legros, and P. Colinet, J. Fluid Mech. **527**, 303 (2005).
[51] C. Ruyer-Quil and P. Manneville, Eur. Phys. J. B **6**, 277 (1998).
[52] C. Ruyer-Quil and P. Manneville, Eur. Phys. J. B **15**, 357 (2000).
[53] C. Ruyer-Quil and P. Manneville, Phys. Fluids **14**, 170 (2002).
[54] S. Kalliadasis, A. Kiyashko, and E. A. Demekhin, J. Fluid Mech. **475**, 377 (2003).